

Accepted Manuscript

Coumarin-indole conjugate donor-acceptor system: Synthesis, photophysical properties, anion sensing ability, theoretical and biological activity studies of two coumarin-indole based push-pull dyes

Tuğçe Aksungur, Burcu Aydınler, Nurgül Seferoğlu, Müjgan Özkütük, Leyla Arslan, Yasemin Reis, Leyla Açık, Zeynel Seferoğlu

PII: S0022-2860(17)30860-8

DOI: [10.1016/j.molstruc.2017.06.079](https://doi.org/10.1016/j.molstruc.2017.06.079)

Reference: MOLSTR 23965

To appear in: *Journal of Molecular Structure*

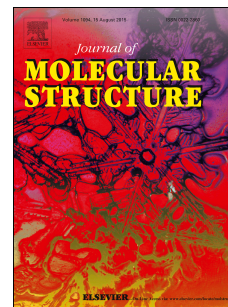
Received Date: 12 May 2017

Revised Date: 15 June 2017

Accepted Date: 17 June 2017

Please cite this article as: Tuğç. Aksungur, B. Aydınler, Nurgü. Seferoğlu, Mü. Özkütük, L. Arslan, Y. Reis, L. Açık, Z. Seferoğlu, Coumarin-indole conjugate donor-acceptor system: Synthesis, photophysical properties, anion sensing ability, theoretical and biological activity studies of two coumarin-indole based push-pull dyes, *Journal of Molecular Structure* (2017), doi: 10.1016/j.molstruc.2017.06.079.

This is a PDF file of an unedited manuscript that has been accepted for publication. As a service to our customers we are providing this early version of the manuscript. The manuscript will undergo copyediting, typesetting, and review of the resulting proof before it is published in its final form. Please note that during the production process errors may be discovered which could affect the content, and all legal disclaimers that apply to the journal pertain.





ACCEPTED

**Coumarin-indole conjugate donor-acceptor system:
Synthesis, photophysical properties, anion sensing ability,
theoretical and biological activity studies of two coumarin-
indole based push-pull dyes**

Tuğçe Aksungur^a, Burcu Aydın^a, Nurgül Seferoğlu^b, Müjgan Özkütük^c, Leyla Arslan^d,
Yasemin Reis^d, Leyla Açıık^d and Zeynel Seferoğlu^{a,*}

^a*Gazi University, Department of Chemistry, 06500 Ankara, Turkey*

^b*Gazi University, Advanced Technology Department, Inst. Sci. & Technol., Ankara, Turkey*

^c*Eskişehir Osmangazi University, Department of Chemistry, 26480 Eskişehir, Turkey*

^d*Gazi University, Department of Biology, 06500 Ankara, Turkey*

Abstract

Two coumarin-indole conjugate fluorescent dyes having donor-acceptor-donor (D-A-D) (**CI-1** and **CI-2**) were synthesized, and characterized using IR, ¹H/¹³C NMR and HRMS. The absorption and emission properties of the dyes were determined in different solvents. The anion sensitivity and selectivity of the dyes were studied with some anions (CN⁻, F⁻, AcO⁻, Cl⁻, Br⁻, I⁻, HSO₄⁻ and H₂PO₄⁻) in DMSO, and their interaction mechanisms were evaluated by spectrophotometric and ¹H NMR titration techniques. In addition, the molecular and electronic structures of **CI-1**, as well as the molecular complexes of **CI-1**, formed with the anions (F⁻ and AcO⁻), were obtained theoretically and confirmed by DFT and TD-DFT calculations. **CI-1** behaves as a colorimetric chemosensor for selective and sensitive detection of CN⁻ in DMSO/H₂O (9:1) over other competing anions such as F⁻ and AcO⁻. However,

only CN^- interacts with chromophore **CI-2** via Michael addition and the main absorption maxima shifts hypsochromically with an observed distinctive color change from orange to yellow. For using as a optic dye, the thermal stability properties of the dyes was determined by TGA (Thermal Gravimetric Analysis). Antimicrobial, antifungal and DNA-ligand interaction studies of the dyes were also examined. The dyes cause conformational changes on DNA and selectively bind to nucleotides of A/A and G/G.

Keywords: Coumarin-indole conjugate, push-pull dye, selective CN^- detection, NLO, DFT, TD-DFT, Biological activity.

*Corresponding authors Tel.: +90 312 2021525; fax: +90 312 2122279

*E-mail addresses: znseferoglu@gazi.edu.tr (Z. Seferoğlu).

1. Introduction

Compounds containing coumarin core represent one of the most important chemical classes of organic fluorescent materials [1]. Many dyes, based on coumarin ring system, have been particularly used in the field of medical diagnostic [2], optoelectronics [3–5], optical whitening [6], cellular imaging [7], fluorescent probes for proteins, amino acids, and for sensing anions/cations [8-14].

Recently, many organic dyes having absorption and emission in the near infrared (NIR) region have attracted continuous attention due to their various applications in biological system, advanced materials and their related fields [15-19]. Some of their advantages include minimal interfering absorption and fluorescence in biological samples, inexpensive laser diode excitation, reduced scattering and enhanced tissue penetration depth. Electron donating

and accepting groups attached in a fluorophore or chromophore can affect optical responses, corresponding shifts of absorption and emission maxima, or fluorescence quantum yields. Generally, the some of fluorescent coumarin derivatives show absorption in the UV region and emit blue light however, the coumarin derivatives bearing donor-acceptor substituents or rings are yellow dyes emitting a green fluorescence. In addition, the most widely used commercial coumarin dyes are fluorescence dyes which contain an electron releasing group such as *N,N*-diethylamino group in the 7-position of the coumarin ring, and in the 3-position, a heterocyclic electron-acceptor residue [20,21]. To shift maximum absorption and emission wavelength of coumarin dyes from UV region to near IR, some researchers synthesized coumarin dyes containing cyano group, dicyanomethine, dicyanomethine vinyl moiety, carbonylvinyl or heterocyclic ring such as benzoxazole, bezothiazole, benzimidazole as electron acceptor in 3- or 4-position, rigid or free rotated alkylamino substituent at 7-position of the main core [22-25]. Moreover, fluorescent bis-coumarin analogues were synthesized having donor-acceptor-donor (D-A-D) system as red and NIR emitting dyes [26]. These types of coumarin derivatives can be applied in many fields such as biolabeling, chemosensor, NLO, etc. Furthermore, coumarins are also of considerable biological and medical interest heterocyclic ring [27-38].

On the other hand, The anion/cation and biological important molecules such as enzymes, proteins, amino acids etc. play a critical role in many metabolic processes. Therefore, determination of anion/cation or biological important analytes with dyes have become a highly hot topic of interest to Organic and Supramolecular chemists [39-61].

The determination of anions can be achieved by several methods including spectroscopic, chromatographic, electrochemical and analytical techniques. However, for practical applications need to simpler methods with minimal instrumental assistance. Colorimetric and fluorimetric chemosensors can be alternative instead of the traditional methods for practical

application in real sample. Therefore, the development of chromogenic chemosensors for anions and cations recognition has become an attractive research field and synthesis of new additional chemosensor is still required.

In view of the above mentioned findings, in this present work, we report synthesis, photophysical, NLO, anion sensing ability, thermal stability, and biological activity of two novel coumarin-indole conjugate donor-acceptor-donor (D-A-D) compounds (**CI-1** and **CI-2**), in which a 7-diethylaminocoumarin donating group, dicyanomethylene moiety, as electron acceptors, linked by an electron donor indole moiety, via vinylene (dimethine) bridge. The photophysical properties and anion sensing abilities of the dyes were evaluated with DFT and TD-DFT.

2. Experimental

2.1. Materials and instrumentation

All the chemicals used in the synthesis of the compounds were procured from the Aldrich Chemical Company and used without further purification. The solvents used were of spectroscopic grade. FT-IR (ATR) spectra were recorded on Perkin-Elmer Spectrum 100 FT-IR spectrophotometer (ν , are in cm^{-1}). NMR spectra were recorded on a Bruker Avance 300 Ultra-Shield in $\text{DMSO-}d_6$. Chemical shifts are expressed in δ units (ppm). Ultraviolet-visible (UV-vis) absorption spectra were recorded on Shimadzu Corporation, Kyoto Japan UV-1800 240V spectrophotometer (Gazi University Department of Chemistry, Turkey) at the wavelength of maximum absorption (λ_{max} , in nm) in the range of the dielectric constant of the solvents, i.e. Dimethylsulfoxide (DMSO, ϵ , 46.45), *N,N*-Dimethylformamide (DMF, ϵ , 36.71), Dichloromethane (CH_2Cl_2 , ϵ , 8.93), Tetrahydrofurane (THF, ϵ , 7.58), Dioksan (ϵ ,

2.21). Fluorescence spectra were also recorded on a HITACHI F-7000 FL Spectrofluorophotometer, in the same range of the same solvents. The slit width was 5 nm for excitation and 5 nm emission. The PMT voltage was 700 V for each measurement. Mass spectra were recorded on Waters-LCT-Premier-XE-LTOF (TOF-MS) instruments; in m/z (rel. %) (Gazi University Laboratories, Department of Pharmacological Sciences). Chemical shifts are expressed in δ units (ppm) with tetramethylsilane (TMS) as the internal reference. Coupling constant (J) is given in hertz (Hz). Signals are abbreviated as follows: singlet, s; doublet, d; triplet, t, and multiplet, m. Melting points were measured on Electrothermal IA9200 apparatus and uncorrected. Thermal analyses were performed with a Shimadzu DTG-60H system, up to 600 °C (10 °C min⁻¹) under a dynamic nitrogen atmosphere (15 mL min⁻¹). Typically, aliquots of a freshly prepared standard solution of the alkylammonium salt of the anions (F⁻, Cl⁻, Br⁻, I⁻, AcO⁻, CN⁻, HSO₄⁻ and H₂PO₄⁻) were added, and their various UV-vis spectra were recorded. ¹H NMR titrations were carried out in DMSO-*d*₆ solution.

2.2. Synthesis and characterization

2.2.1. Synthesis of (2)

3.40 mmol of indole-3-carbaldehyde was dissolved in 5 mL of distilled DMF. Then, 3.4 mmol of K₂CO₃ and 1 mL CH₃I were added over it and stirred thoroughly. The mixture was boiled under nitrogen at 100 °C for 5 hours under reflux. The solution obtained after 5 hours was cooled, precipitated with ice-water, and filtered. White solid, yield: 61% (0.33 g), m.p: 62 °C, ¹H NMR (DMSO-*d*₆, 300 MHz): 9.9 (s, 1H), 8.29 (s, 1H), 8.1 (d, 1H, $J=7.24$), 7.57(d, 1H, $J=8.014$), 7.3 (dd, $J=7.09, 1.15$), 7.4 (dd, $J=5.82, 4.61$).

2.2.2. Synthesis of 3-acetyl-7-(diethylamino)-2H-chromen-2-one (**3**) and 2-1-(7-(diethylamino)-2-oxo-2H-chromen-3-yl)ethylidene)malononitrile (**4**)

Compounds **3** and **4** were synthesized by our previously reported procedures [62].

2.2.2. General procedure for the preparation of (E)-2-(1-(7-(diethylamino)-2-oxo-2H-chromen-3-yl)-3-(1H-indol-3-yl)allylidene)malononitrile (**CI-1**), and (E)-2-(1-(7-(diethylamino)-2-oxo-2H-chromen-3-yl)-3-(1-methyl-1H-indol-3-yl)allylidene)malononitrile (**CI-2**)

A mixture of 2-(1-(7-(diethylamino)-2-oxo-2H-chromen-3-yl)ethylidene)malononitrile (**3**) (10 mmol), piperidine (1 mmol), and indole-3-carbaldehyde, or 1-Methyl-1H-indole-3-carbaldehyde (10 mmol), in ethanol (20 mL) was refluxed for 18 hours. After cooling to room temperature, the precipitate was filtered and dried. The crude product was recrystallized from ethylacetate to obtain the pure compound, in both cases, as fine red powder.

(CI-1): Yield 50% (0.22 g); mp: 282-283 °C. FT-IR (ATR, ν_{\max} , cm^{-1}): 3256 (N-H) 2979, 2925 (aliphatic C-H), 2212 (C \equiv N), 1705 (C=O), 1569 (aromatic C=C), 1331 (aromatic C-N), 1236 aliphatic C-N); ^1H NMR (DMSO- d_6 , 300 MHz): 12.25 (brs, N-H), 8.14 (s, 1H), 8.08 (s, 1H), 7.83 (dd, 1H, $J = 6.36, 2.63$ Hz), 7.68 (d, 1H, $J = 15.17$), 7.51 (m, 1H), 7.35 (d, 1H, $J = 7.05$ Hz), 7.28 (m, 3H), 6.80 (dd, 1H, $J = 8.74, 2.35$), 6.64 (d, 1H, $J = 2.19$), 3.50 (q, 4H, $J = 7.15$) 1.27 (t, 6H, $J = 7.14$) ppm; ^{13}C NMR (DMSO- d_6 , 75 MHz): 194.5, 185.6, 184.2, 179.0, 165.2, 151.8, 142.1, 141.5, 139.3, 134.5, 101.2, 71.5, 67.6, 67.30, 66.9, 66.3, 66.0; HRMS (ESI, CH_3CN) ($\text{C}_{27}\text{H}_{22}\text{N}_4\text{O}_2$) found: 435.1831, calcd.: 435.1821.

(CI-2): Yield 60% (0.27 g); mp: 271-272 °C, FT-IR (ATR, ν_{\max} , cm^{-1}): 2971 (aliphatic C-H), 2210 (C \equiv N), 1705 (C=O), 1566 (aromatic C=C), 1329 (aromatic C-N), 1235 aliphatic C-N),

^1H NMR (DMSO- d_6 , 300 MHz): 8.14 (s, 1H), 8.08 (s, 1H), 7.83 (dd, 1H, $J = 5.64, 2.20$ Hz), 7.68 (d, 1H, $J = 15.19$), 7.51 (m, 1H), 7.35 (d, 1H, $J = 8.95$ Hz), 7.28 (m, 3H), 6.80 (dd, 1H, $J = 8.98, 2.24$), 6.64 (d, 1H, $J = 2.16$), 3.89 (s, 3H), 3.50 (q, 4H, $J = 7.15$) 1.27 (t, 6H, $J = 7.14$) ppm; ^{13}C NMR (DMSO- d_6 , 75 MHz): 194.5, 185.6, 184.2, 179.0, 165.2, 151.8, 142.1, 141.5, 139.3, 134.5, 101.2, 71.5, 67.6, 67.30, 66.9, 66.3, 66.0; HRMS (ESI, CH_3CN) ($\text{C}_{27}\text{H}_{22}\text{N}_4\text{O}_2$) found: 449.1962, calcd.: 449.1978.

Scheme 1 is here

3. Results and discussion

3.1. Synthetic strategy and structural characterization

The syntheses of **CI-1** and **CI-2** were performed by stepwise procedure demonstrated in **Scheme 1**. The reaction of 2-(1-(7-(diethylamino)-2-oxo-2H-chromen-3-yl)ethylidene)malononitrile (**4**) with indole-3-carbaldehyde (**1**) and 1-methylindole-3-carbaldehyde (**2**) in the presence of piperidine gave *E*-2-(1-(7-(diethylamino)-2-oxo-2H-chromen-3-yl)-3-(1H-indol-3-yl)allylidene)malononitrile (**CI-1**), and *E*-2-(1-(7-(diethylamino)-2-oxo-2H-chromen-3-yl)-3-(1-methyl-1H-indol-3-yl)allylidene)malononitrile, respectively. The structures of both compounds were confirmed by FT-IR, UV-vis, ^1H NMR, ^{13}C NMR and HRMS techniques. The spectral data were consistent with the proposed structures (**Supplementary material Figs. S1-9**).

The FT-IR spectra of the prepared dye **CI-1** showed two characteristic bands at 3256 and 1705 cm^{-1} , corresponding to amine (N-H, belong to indole moiety) and carbonyl (C=O, belong to coumarin moiety), respectively. Dye **CI-2** showed carbonyl (C=O) band at 1705

cm^{-1} . Donor- π -acceptor compounds bearing vinyl bridge can show cis-trans (*E/Z*) isomer in solution. The determination of more stable isomer is quite important for evaluating their photophysical properties. ^1H NMR spectroscopy is useful in the measurement of the configuration of the vinylic double bond. The configuration of the *E*-isomer could be noticed by NMR spectroscopic analysis. The assignment of the *E*-configuration of the vinylic double-bond was based on the analysis of the vicinal coupling constants of the olefinic protons, because the latter exhibit the characteristic coupling constant of $J \sim 15\text{-}16$ Hz. This coupling constant for the vinylic protons of **CI-1** and **CI-2** clearly supports the selective formation of *E*-configuration of the vinylic double-bond. In addition, in the ^1H NMR spectra of **CI-1**, the NH peak was observed at 12.25 ppm in $\text{DMSO-}d_6$.

3.2. Photophysical properties

Recently, many push-pull chromophores have also been used extensively as fluorescent emitters because of their good absorption and fluorescence properties. For examples, Dicyanomethylene-4*H*-pyran (DCM) in particular, is a very well-known red emitter for OLED application [63]. Therefore, in this study DCM-like new chromogenic dyes (**CI-1** and **CI-2**) bearing well-known fluorescent core coumarin, were designed and synthesized as D- π -A type push-pull system. The synthesized dyes consist of 7-diethylaminocoumarin and indole moiety as a donor part and dicyanomethylene at the 3-position of coumarin moiety as an acceptor part in the structure. Generally, the polarity of solvents strongly affects the excited state of the donor-acceptor compounds via stabilize dipole-dipole, hydrogen bonding, and solvation interactions. Therefore, in the present study, the solvent dependent absorption as well as emission behavior of these compounds were evaluated in solvents of various dielectric constants. The effect of solvent polarity on absorption and photoluminescence (PL) properties

of the dyes was studied in five aprotic solvents (DMSO, DMF, CH₂Cl₂, THF and Dioxan in 3x10⁻⁵ M) of various polarity. The UV-vis and photoluminescence (PL) spectroscopic data of compounds **CI-1** and **CI-2** measured in studied solvents at room temperature are presented in **Table 1**. Effects of solvent polarity on absorption and emission spectra of the dyes, and the color changes observed in day light, upon UV irradiation (365 nm) of compounds in diverse solvents, are shown in **Fig.1.** and **Fig.2.**

Dyes **CI-1** and **CI-2** displayed solvatochromic properties in all the solvents. They also showed red shifted absorption with increase in solvent polarity that is for CH₂Cl₂ (λ_{abs} is 446 nm and 461 nm, for **CI-1** and **CI-2**, respectively), for DMSO (λ_{abs} is 470 nm and 477 nm, for **CI-1** and **CI-2**, respectively) (**Fig. 1, Table 1**). One dominant absorption band at a long wavelength with a shoulder at short wavelength was observed in all solvents used for both dyes. Any of the dyes which has one absorption band with shoulder, may exhibit *E-Z* isomerization. In addition, **CI-1** showed one additional absorption maximum at long wavelength in DMF. This maximum absorption wavelength can be attributed to anionic form of the dye.

In push-pull dipolar molecules have been seen photoinduced charge transfer with characteristic absorption band. In this study, it was found that the maximum absorption shifted from 446 nm to 461 nm when CH₃ is attached to the indole ring as electron-donating substituent, in CH₂Cl₂. This result is in agreement with the assumption of intramolecular charge transfer (ICT), and an ICT enhancement results in the bathochromic shift of the absorption bands. The same behaviour was observed for the rest of the solvents used.

The emission spectra were obtained using 5 nm slit width, and 10 mM stock solute concentration, by exciting the samples at its wavelength of emission maxima and the results obtained are summarized in **Table 1**. There was no regular correlation between the change of solvent polarity and emission maxima. It was observed that the change in solvent polarity did

not have significant influence on emission curve (**Fig.1, Table 1**). However, the fluorescence intensity of the compounds decreased with the increasing polarity of the solvents, which is different from the common results in the emission intensity of ICT compounds such as styryl dyes [64]. It may be due to the stabilization of the excited state in polar solvent environment leading to quenching of fluorescence intensity which suggests that there is positive solvatochromism with negative solvatofluorism [65]. The largest Stokes shifts were observed in CH_2Cl_2 (151 nm) for the chromophores.

Table 1 is here

Figures 1a and 1b are here

3.2. UV-vis absorption titration of CI-1 and CI-2 with various anions

The anion binding and the sensing ability of the novel push-pull dyes **CI-1** and **CI-2** were performed in DMSO using spectrophotometric and spectrofluorimetric titration techniques. Aprotic, polar and water miscible DMSO was chosen as the solvent for anion titrations to avoid anion-solvent interactions. The anion titrations were performed with different molar equiv of TBA salts of anions. **Fig.3** shows the changes in the absorption spectrum of **CI-1** (2×10^{-5} M) in DMSO in the absence and the presence of F^- , AcO^- and CN^- anions at room temperature. The main band of **CI-1** dye observed at 466 nm decreased gradually, and upon adding F^- anion, an increased and a new absorption maximum was observed at 530 nm. The color change of the dye was also observed by the naked eye, simultaneously, from yellow to red in the presence of F^- (see **Fig. 4**). An isosbestic point was observed at 497 nm during the titration process, indicating that a stable binding complex was formed between receptor **CI-1** and fluoride anion. As shown in **Fig.3**, titration profile of **CI-1** with F^- found to be 40 equiv

of F^- reacting with **CI-1** could reach equilibrium. Which indicated that the dye interact with F^- by hydrogen bonding at solution phase and deprotonated during addition of fluoride ion. This result shows that a ground-state equilibrium between neutral **CI-1** and deprotonated **CI-H⁺** has been formed, which can be attributed to an indole moiety (**Scheme 2**). In this form, the negative charge on the indole nitrogen is completely delocalized, leading to the experimentally observed bathochromic shift at 530 nm, as compared to the neutral form. The optical response on interaction with F^- can be explained by the fact that ICT process occurred between the indole nitrogen and the electron-withdrawing dicyanomethylene with the formation of a hydrogen bonded complex between the F^- of chemosensor and the anion added. The same spectral response towards AcO^- and CN^- anions was observed as shown in **Fig. 3**.

Figure 4 is here

We investigated the reversibility of the anions sensing upon addition of trifluoroacetic acid (TFA) in fluoride titrated **CI-1** solution. The absorption spectral change of **CI-1-H⁺** with the addition of TFA in DMSO solution is shown in **Fig. 5** and **Scheme 2**. Addition of 40 equiv of TFA to a solution of **CI-1-H⁺**, resulted in the disappearance of the absorption bands at 533 nm. Again, a new absorption maximum was observed at a shorter wavelength with the same absorption maximum at 466 nm of the neutral form, upon addition of 40 equiv of TFA.

Figure 5 is here

Scheme 2 is here

The addition of F^- and CN^- resulted in a yellow-to-pink colour change, whereas a yellow-to-orange colour change was observed in the case of AcO^- (**Fig.4**). No considerable color changes were seen when Cl^- , Br^- , I^- , HSO_4^- and $H_2PO_4^-$ ions were added, which was consistent with the results observed from spectral titrations (**Supplementary material Figs. S10-12**).

We carried out the sensing test of **CI-1** to test for anions in the water. Because the anion affinity may be changed if the same experiment is carried out in aqueous medium due to the hydration of the anions by water. The detection of anions in real samples was also simulated by using DMSO/ H_2O binary solution. Indeed, when chemosensor **CI-1** was treated with the some selected anions; F^- , AcO^- and CN^- (25 equiv of each) in DMSO/ H_2O (9:1) binary solution, there was a distinctive absorption maximum change with CN^- only (**Fig.6**). Upon addition of CN^- to the receptor, the absorption maximum of **CI-1** shifted bathochromically. This phenomenon was observed upon addition of CN^- only. However, the new color changes, which can be observed by the naked-eye, are not the same as the previous ones because of the differences in the solution environment. The chemosensor **CI-1** displayed a color change from yellow to red. However, no significant color change was observed upon addition of F^- and AcO^- (**Fig.7**).

Figures 6 and 7 are here

CI-2 has no acidic hydrogen and is composed of a 7-diethylaminocoumarin fluorophore, and a dicyanomethylene moiety, as strong electron acceptor linked to the indole moiety via dimethine, and for activating the Michael acceptor for cyanide anion. Such a molecular design makes probe **CI-2** possess the expanded π -conjugation as well as the strong ICT from the indole to the conjugated dicyanomethylene moiety, which will lead to the red absorption

maximum. Upon addition of CN^- , the absorbance at 476 nm gradually decreased with a new peak appearing at 391 nm. 20 equiv of cyanide was sufficient to drive the reaction to completion. It is expected that cyanide anion can add to the δ -position of an activated Michael acceptor to generate the stabilized anionic species **CI-2-CN⁻**. Apparently, after addition of CN^- , it leads to the collapse of the donor-acceptor system, and a hypsochromic shift of absorption maxima was observed (**Fig.8**). As a result, the π -conjugation between indole/coumarin and dicyanomethylene was blocked and then obvious spectra and color changes were observed. The same hypsochromic shifts were also observed for coumarin based donor-acceptor dyes [66,67]. In addition, upon addition of CN^- to a solution of **CI-2**, an obvious color change from orange to yellow was clearly observed (**Fig.9**). No considerable color changes were seen when F^- and AcO^- ions were ratiometrically added to the solution of **CI-2**. As a result, a ratiometric colorimetric response, as well as an obvious color change could be expected. Therefore, **CI-2** can serve as cyanide sensor.

Figures 8 and 9 are here

3.3. ¹H NMR titrations study

The results from spectrophotometric titration clearly showed that probe **CI-1** associates with AcO^- and F^- via a hydrogen bonding interaction between the indolic acidic NH proton of **CI** and AcO^- and F^- . The interaction between the probe with CN^- showed that there is a different mechanism beside deprotonation. To gain an insight into the nature of the ground interaction between **CI-1** and F^- , we recorded the ¹H NMR spectra of the probe in DMSO solution without, and with added TBAF in $\text{DMSO-}d_6$. As shown in **Fig. 10**, addition of just 1 equiv of TBAF resulted in the complete disappearance of the NH signal of the probe at 12.25 ppm,

while a new broad signal, attributable to the formation of HF_2^- complex, was observed at δ 16.0 ppm after addition of 8 equiv F^- because of proton transfer from N-H to F^- . After deprotonation of indol NH, electron density on indol moiety and ICT from indol donor to dicyanomethylene acceptor increase and thus some protons can shift upfield. The shielding effect of the negatively charged indole ring is an evident of the upfield shifts of the aromatic proton at the 2-position of the indol ring (Hb) upon the addition of 8 equiv of F^- to the solution of **CI-1**. In addition, the negative charge shift also promotes upfield shift of the vinylic CH protons (i.e. Hc and Hd) which shifted slightly upfield, upon addition of same amount of F^- to the solution of **CI-1**.

The AcO^- ion is basically a competing anion with F^- ion. However, the same behavior was observed in AcO^- ion when it was interacted with the probe in DMSO solution. With the addition of 9 equiv of AcO^- to the solution of **CI-1**, deprotonation probably occurred, which led to an increase in the electron density on the indole heterocyclic ring (**Supplementary material Fig. S13**).

Figure 10 is here

CN^- is different from F^- and AcO^- when the receptor affinity is taken into account. Therefore, we evaluated its interaction mechanism with the compounds, and **CI-2** has been chosen as the model compound instead of **CI-1**. This is because **CI-2** has no any acidic hydrogen and only nucleophilic addition with CN^- will be observed. To further understand the mechanisms between CN^- and **CI-1**, and also CN^- and **CI-2**, both compounds were titrated with CN^- . Upon addition of 6 equiv of CN^- to the solution of **CI-1**, Ha and Hb signals which were at 8.14 and 12.25 ppm respectively, disappeared. While Ha signal disappearance indicates the deprotonation of NH proton, Hb signals suggest cyanide addition to carbon at 2-position of

the indole ring. For confirmation of this mechanism we did the same with **CI-2** which doesn't have acidic NH proton for deprotonation. Within the addition of 2 equiv of CN^- to the solution of **CI-2**, Hb proton as was expected disappeared, and the He at 3-position of coumarin ring at 8.08 ppm, also disappeared. However, for Hg and Hh at 6 and 8-position respectively, of the coumarin ring, their signals were shifted upfield. This results indicates that, beside the addition of cyanide to 2-position of the indol ring, there is also an addition to 4-position of coumarin ring.

All the observed differences on the proton signals of **CI-1-CN** adduct suggest that, two different mechanisms (deprotonation and addition) occur at the same time in ^1H NMR titration for **CI-1**, but at the end of the titration, the major product was produced by the deprotonation reaction (**Fig. 11**). In addition, ^1H NMR of **CI-2-CN** adduct showed that, CN^- was added at the 4-position of the coumarin, and 2-position of the indol ring, via nucleophilic addition reaction (**Fig. 12**).

Figures 11 and 12 are here

The ground state geometry of the synthesized dyes was optimized within a framework of Gaussian 09 [68] using the density functional theory (DFT) method. The calculations were performed using the Becke's three-parameter exchange function with the Lee–Yang–Parr correlation function (B3LYP) [69-71] applying the 6-31+G(d,p) basis set without any symmetry restrictions in the gas phase. The harmonic vibrational frequency calculations using the same methods, as that of the geometry optimizations, were used to ascertain the presence of a local minimum. The vertical excitation energies and oscillator strengths were obtained for the lowest 10 singlet-singlet transitions at the optimized ground state equilibrium geometries, by using TD-DFT at the same hybrid functional and basis, set in CH_2Cl_2 , dioxan, DMF, DMSO, THF solutions using the polarizable continuum model (PCM) [72]. Besides,

detailed information about absorption changes, upon the reactions of F^- and AcO^- with **CI-1**, were obtained using DFT and TD-DFT calculations and were parallel to the experimental results. In addition, nonlinear optical properties, the electric dipole moment (μ), polarizability (α), anisotropy of polarizability ($\Delta\alpha$) and molecular first hyperpolarizability (β) of the molecules were evaluated in the gas phase.

3.4.1. Electronic properties

The calculated vertical excitation energies and oscillator strengths obtained for the lowest energy transition with transitions with highest orbital contributions for **CI-1** and **CI-2** (**Fig. 13**) are presented in **Table 2**. As seen in the Table, the calculated values are in good agreement with the experimental ones. In all solvents, the absorption bands of both **CI-1** and **CI-2** molecules consist of two peaks ($\lambda_{max}= 439, 378$ nm in CH_2Cl_2 , $\lambda_{max}= 434, 368$ nm in dioxan, $\lambda_{max}= 441, 380$ nm in DMF, $\lambda_{max}= 441, 380$ nm in DMSO, $\lambda_{max}= 438, 377$ nm in THF for **CI-1**, $\lambda_{max}= 447, 377$ nm in CH_2Cl_2 , $\lambda_{max}= 431, 368$ nm in dioxan, $\lambda_{max}= 449, 380$ nm in DMF, $\lambda_{max}= 448, 380$ nm in DMSO, $\lambda_{max}= 446, 376$ nm in THF for **CI-2**). When we compared the calculated values with the experiment ones, it was seen that the largest difference in λ_{max} , between each of the two peaks, was 29 nm in DMSO for both **CI-1** and **CI-2**. On the other hand, the absorption maxima of **CI-2** is slightly red shifted as compared to that of **CI-1** because of the addition of electron-donating group (CH_3) at the 1-position of indole. In addition, the TD-DFT calculations showed that, the main transition at high wavelength corresponds to HOMO-1 \rightarrow LUMO transition, and the other at low wavelength corresponds to HOMO \rightarrow LUMO+1 for **CI-1** and **CI-2**.

Figure 13 and Table 2 are here

3.4.2. Sensing mechanism of **CI-1**

In parallel to experimental study, to get further understanding on the interaction of **CI-1** with F^- and AcO^- anions, we optimized the structure of **CI-1** complexes with F^- and AcO^- in gas phase as shown in **Fig. 13**. The optimized structures of **CI-1** and its complexes with F^- and AcO^- anions (**CI-1+ F^-** , **CI-1+ AcO^-**) in gas phase are shown in **Fig. 13**. It was observed that, the amide NH bond length of **CI-1** increased from 1.008 Å to 1.507 Å, and then to 1.136 Å upon its interaction with F^- and AcO^- anions, respectively, through hydrogen bonding, which was followed by deprotonation process. The comparison of the Mulliken's atomic charges on nitrogen atom of indole for the optimized structures showed the change from -0.275 to -0.354, and -0.285 after the formation of **CI-1+ F^-** and **CI-1+ AcO^-** complexes, respectively. The increased negative charge caused an enhanced ICT within the molecule and decreasing the energy gap between HOMO and LUMO (HOMO for the highest occupied molecular orbitals, LUMO for the lowest unoccupied molecular orbitals) resulting in red shift, which is in accordance with the observed absorbance spectra.

To get detailed information about the absorption spectra of **CI-1**, **CI-1+ F^-** , and **CI-1+ AcO^-** , the TD-DFT (time-dependent density functional theory) calculations were carried out at B3LYP/6-31+G(d,p) level in DMSO at the optimized geometries. For **CI-1**, the TD-DFT calculations showed main transition at 441 nm with an oscillator strength of $f = 0.7430$ which corresponds to HOMO-1→LUMO transition, and the other at 380 nm with $f = 0.5863$ which corresponds to HOMO-1→LUMO+1 (6.6%) and HOMO→LUMO+1 (89.7%) transitions.

When **CI-1** formed a complex with F^- , the absorption peak appeared at 518 nm, red-shifted by 77 nm, which is in good agreement with the experimental absorption change of 67 nm. The AcO^- interaction with **CI-1** resulted in similar behavior as seen in **CI-1+ F^-** and the peak appeared at 520 nm, red-shifted by 79 nm compared with **CI-1**. These observed absorption

maxima of **CI-1+F⁻** and **CI-1+AcO⁻** were found to correspond to HOMO→LUMO (contribution is 92.5% for **CI-1+F⁻**, 71.6% for **CI-1+AcO⁻**) and HOMO-1→LUMO (5.6% for **CI-1+F⁻**, 27.8% for **CI-1+AcO⁻**). The molecular orbitals that are relevant to the excitations for **CI-1** and **CI-1+F⁻** and **CI-1+AcO⁻** are given in **Fig. 14**. It is seen that HOMO and LUMO orbitals of **CI-1+F⁻** and **CI-1+AcO⁻** are mainly delocalized on the donor indole moiety and acceptor dicyanomethylene through π -bond conjugation. After excitation from HOMO to LUMO, ICT occurs from indole moiety on the donor to the acceptor end, resulting in the fluorescence quenching. The results obtained from calculations were in good agreement with the experimental results.

Figure 14 is here

3.4.3. Molecular Electrostatic Maps (MEP)

MEP is highly useful in predicting the reactive behavior of molecules. To predict reactive sites for the electrophilic and nucleophilic process for **CI-1** and **CI-2**, MEP surface was obtained at the B3LYP/6-31+G(d,p) optimized geometry shown in **Fig.15**. The negative (red and yellow) regions of MEP were related to electrophilic reactivity and the positive (blue) ones to nucleophilic reactivity. As seen in MEP map of **CI-1** in **Fig.15**, N-H bond indicates a possible site for attack of anions. It gives an information about the region where the molecule can have intermolecular interactions.

3.4.4. Nonlinear Optical Properties (NLO)

Nonlinear optics (NLO) deals with the interactions of applied electromagnetic fields in various materials to generate new electromagnetic fields, altered in frequency, phase and other physical properties [73]. It is known that the investigations of NLO materials have been the subject of intense research because of their possible applications in a wide range of technologies, such as optical communication, optical computing and data storage [72-75].

In this study, the electric dipole moment (μ), polarizability (α_{tot}) and molecular first hyperpolarizability (β_{tot}) of **CI-1** and **CI-2** were calculated at B3LYP/6-31+G(d,p) level in gas phase. The obtained results are given in **Table 3**. As seen in **Table 3**, the values of α_{tot} and β_{tot} were obtained as 65.6×10^{-24} esu and 57×10^{-30} esu for **CI-1**, 68.2×10^{-24} esu and 59.2×10^{-30} esu for **CI-2**. As expected, α_{tot} and β_{tot} for **CI-2** are larger than those for **CI-1** because of the addition of electron-donating group (CH_3) at the 1-position of the indole. On the other hand, the values of α_{tot} and β_{tot} for **CI-1** and **CI-2** were found to be greater than those of urea (α_{tot} and β_{tot} of urea are 4.9×10^{-24} esu and 0.49×10^{-30} esu obtained by B3LYP/6-31+G(d,p) method) which is one of the prototypical molecules used in the study of the NLO properties of molecular systems. The results show that the value of the first hyperpolarizability (β_{tot}) are more than ~120 times larger than the magnitude of urea. According to the magnitude of the first hyperpolarizability, the studied compounds may be potential applicants in the development of NLO materials.

3.5. Thermal analysis

The thermal stability of the dyes **CI-1** and **CI-2** has a fundamental characteristic deciding their suitability for applications as functional dyes in many fields such as chemosensors and

as optic dyes. Dyes **CI-1** and **CI-2** were used to carry out thermal gravimetric techniques (TGA). The thermo gravimetric studies were conducted at 30-600 °C under nitrogen gas at a heating rate of 10 °C min⁻¹. The TGA result indicated that **CI-1** has two thermal decomposition temperatures (T_d) 160 °C and 299 °C. **CI-1** is stable up to 160 °C, and lost 88% weight at that temperature, as shown in **Fig. 16**. TGA revealed the onset decomposition temperature (T_d) at 299 °C for **CI-1** whose thermogravimetric curve showed a major loss in weight. However, **CI-2** was found to be more stable than **CI-1**, and there was no decomposition band till at 325 °C. As a results, the dyes showed good thermal stabilities approximately up to 300 °C, which is high enough for industrial applications when use as chemosensors or optic dyes.

Figure 16 is here

3.6. *In vitro* antimicrobial activity

The antimicrobial activity of the compounds (**CI-1** and **CI-2**) were tested against both types of Gram-positive (*Bacillus cereus* NRRL B-3711, *Bacillus subtilis* ATCC 6633, *Staphylococcus aureus* ATCC 25923, *Enterococcus faecalis* ATCC 29212) and Gram-negative bacteria (*Escherichia coli* ATCC 35218, *Escherichia coli* ATCC 25922, *Pseudomonas aeruginosa* ATCC 27853, *Klebsiella pneumoniae* ATCC 13883, *Salmonella typhimurium* ATCC 14028) and fungi (*Candida albicans* ATCC 10231, *Candida krusei* ATCC 6258, *Candida tropicalis* Y-12968). Microorganism strains used were obtained from the collections of Gazi University Molecular Biology Culture Collection, Turkey. For comparison, ampicillin (10 µg), chloramphenicol (30 µg), (antibacterial) and ketoconazole (50 µg), (antifungal) were used as the standard antimicrobial agents. Test strains were

incubated on nutrient agar plates at 37 °C for 24 h for bacteria. The yeast cells were cultured on Sabouraud dextrose agar medium and incubated at 30 °C for 48 h. After incubation, bacterial suspensions were adjusted to a turbidity of 0.5 McFarland. Mueller Hinton agar (for bacterial strains) and sabouraud dextrose agar (for fungal strains) mixed with 1% culture suspension and poured into the plates. Wells were prepared with a 6.0 mm diameter and the solution (50 µL) of the 5000 µM test compound was poured into the well. The diameter of the inhibition zone was measured in millimeters.

The antimicrobial activity of the compounds **CI-1** and **CI-2** were evaluated against nine bacterial and three fungal test strains (**Table 4**). Compound **CI-1** had slightly inhibitory effect on *E. coli*, *P. aeruginosa*, *K. pneumoniae*, *S. typhimurium* bacterial species, and moderate effect on *C. albicans* yeast species. On the other hand, compound **CI-2**, had quite strong antifungal activity against pathogenic candida species of *C. krusei*, *C. albicans* and *C. tropicalis*. Minimal Inhibitory Concentrations and Minimal Fungicidal Concentrations are the lowest concentration of a chemical that prevents visible growth of a microorganism and is the lowest concentration of an antifungal agent to kill particular fungi, respectively. The MIC and MFC values of the compounds are given in **Table 5**. MIC values ranged from 10-80 µM, whereas MFC ranged from 20-80 µM.

Tables 4 and 5 are here

3.7. The DNA interaction with the compounds (CI-1 and CI-2)

The interaction of the synthesized compounds with plasmid DNA was studied by agarose gel electrophoresis. Stock solutions of the compounds in DMSO were prepared and used immediately. The aliquots of decreasing concentrations of the compounds, ranging from 150 to 3.125 μM , were incubated with plasmid DNA in the dark at 37 °C for 24 h. The loading buffer (0.1 % bromophenol blue, 0.1 % sucrose) was added to the mixtures and loaded onto the 1% agarose gel. Electrophoresis was carried out under TAE buffer (0.05 M Tris base, 0.05 M glacial acetic acid and 1 mM EDTA, pH=8.0) for 3 h at 70 V. The gel was stained with ethidium bromide (0.5 $\mu\text{g}/\text{mL}$), visualized under UV light using a transilluminator (BioDoc Analyzer, Biometra) and the image was captured with a video camera as a TIFF file. The experiments were repeated three times, and the mean values were presented.

The plasmid DNA was treated with compounds **CI-1** and **CI-2** in the dark at 37 °C for 24 h, and then the mobilities of the DNA forms were studied in an agarose gel electrophoresis. **Fig. 17** shows the electrophoretograms applied to the incubated mixtures of DNA at various concentrations (150 μM -3.125 μM) of the compounds. Lane P applies to the untreated plasmid DNA (control DNA), showing the major supercoiled circular (form I) and minor singly nicked relaxed circular (form II) forms of the plasmid DNA. Lanes 1-7 apply to plasmid DNA incubated with compounds ranging from 150 μM to 3.125 μM .

When the plasmid DNA was incubated with decreasing concentrations of the compounds **CI-1** and **CI-2**, the mobility of form I DNA decreased at three high concentrations, and then increased slightly, In case of form II, the intensity decreased at the first high concentration, then increased slightly with the decreasing concentration of the compounds.

Figure 17 is here

3.8. Determination of nucleotides interacted with the nucleotides

The compounds/plasmid DNA mixtures were incubated for 24 h, and then restricted with *Bam*HI or *Hind*III enzyme at 37 °C in order to determine the nucleotides to which the compound binds. The restricted DNA was run in 1% agarose gel electrophoresis in TAE buffer. The gel was stained with ethidium bromide (0.5 µg/mL), and the gel was then viewed with a transilluminator, while the image was photographed with a video-camera and saved as a TIFF file. **Fig. 18** illustrates the electrophoretogram for the *Bam*HI and *Hind*III digested mixtures of plasmid DNA after their treatment with the compounds. Untreated plasmid DNA was applied to lane 1. Lane 2 applies to plasmid DNA digested with *Bam*HI. Lanes 3-5 apply to plasmid DNA interacted with the compound BT1, and lanes 6-8 apply to plasmid DNA interacted with the compound BT1 followed by their digestions with *Bam*HI and *Hind*III. In case of digestions of the compounds **CI-1** and **CI-2** with *Bam*HI and *Hind*III, Form I, Form II, and Form III were observed, showing that the compounds bind to A/A and G/G nucleotides.

Figure 18 is here

4. Conclusions

In conclusion, a novel coumarin-indole conjugate push-pull chromophores (**CI-1** and **CI-2**) have been synthesized by Knoevenagel condensation, and characterization by IR, ¹H/¹³C NMR and HRMS. Both dyes are stable *E* isomers that is confirmed by ¹H NMR spectra. The effect of solvent polarity on absorption and emission maxima of the dyes was studied in five aprotic solvents of various polarities was investigated. The dyes displayed solvatochromic properties in all the solvents used.

CI-1 behaved as a colorimetric probe for selective and sensitive detection of F^- , AcO^- and CN^- in a biologically competing solvent like DMSO. However, it showed selective determination of CN^- in DMSO/ H_2O (9:1) over other competing anions such as F^- and AcO^- . This result indicated that **CI-1** could be used as a highly selective colorimetric sensor for CN^- in DMSO/ H_2O (9:1). In addition, when **CI-2** was treated with some selected anions, such as F^- , AcO^- and CN^- , only CN^- reacted with chromophore **CI-2** via Michael addition, and the main absorption maxima shifted hypsochromically, and a distinctive color change was observed from orange to yellow. The TGA result shows that the dyes have an enough thermal stability for applications. Also, this study showed that **CI-2** has potential uses, and can act against the tested fungal strains. In addition, both compounds **CI-1** and **CI-2** exhibited conformational alterations in DNA. It is generally accepted that, DNA is an important and major pharmacological target for drug design. Since DNA is able to adopt a variety of different conformations according to the environmental factors, as well as naturally occurring in different forms, DNA as the plasmid is potentially used to test for antitumor drugs. For example, cisplatin is a well-known antitumor drug and its main target is DNA. It is responsible for the cure of over 90% of testicular cancer [76]. DNA-compound interactions studies are based on mobility and conformations changes of plasmid DNA. Hence, we tried to find out DNA binding mode and the types of nucleotides binding. We concluded that, both compounds **CI-1** and **CI-2** can cause conformational changes on DNA and can selectively bind to nucleotides of A/A and G/G.

Acknowledgements

This work was supported by Gazi University.

Supplementary material

Supplementary data (Copies of ^1H NMR, ^{13}C NMR, HRMS and absorption spectra on anions-chemosensor interactions **Figs. S1–S13**) associated with this article can be found, in the online version, at.....

References

- [1] R.M. Christie, C. Lui, Studies of fluorescent dyes: part 1. An investigation of the electronic spectral properties of substituted coumarins, *Dye Pigm.* 42 (1999) 85-93, doi:[http://dx.doi.org/10.1016/S0143-7208\(99\)00012-1](http://dx.doi.org/10.1016/S0143-7208(99)00012-1).
- [2] R. O'-Kennedy, R. Douglas Thornes (Eds.), *Coumarins: Biology, Applications and Mode of Action*, New York: John Wiley, 1997.
- [3] X. Liu, J.M. Cole, P.G. Waddell, T.C. Lin, J. Radia, A. Zeidler, Molecular origins of optoelectronic properties in coumarin dyes: toward designer solar cell and laser applications, *J. Phys. Chem. A* 116 (2012) 727–737, doi:<http://dx.doi.org/10.1021/jp209925y>.
- [4] F.A. Mir, Optical and Schottky diode performance of Au/4-hydroxy Coumarin/ ITO heterojunction, *Opt. Int. J. Light Electron Opt.* 126 (2015) 24–27, doi:<http://dx.doi.org/10.1016/j.ijleo.2014.07.146>.
- [5] S. Kumar, P. Singh, R. Srivastava, R.R. Koner, A. Pramanik, J. Mathew, S. Sinha, M. Rawat, R.S. Anand, S. Ghosh, Engineering fused coumarin dyes: a molecular level understanding of aggregation quenching and tuning electroluminescence via alkyl chain substitution, *J. Mater. Chem. C* 2 (2014) 6637–6647, doi:<http://dx.doi.org/10.1039/C4TC00807C>.

- [6] S.S. Keskin, N. Aslan, F. Bayrakçeken, Optical properties and chemical behavior of laser-dye Coumarin-500 and the influence of atmospheric corona discharges, *Spectrochim. Acta A Mol. Biomol. Spectrosc.* 72 (2009) 254–259, doi:<http://dx.doi.org/10.1016/j.saa.2008.09.024>.
- [7] G. Signore, R. Nifosì, L. Albertazzi, B. Storti, R. Bizzarri, Polarity-sensitive coumarins tailored to live cell imaging, *J. Am. Chem. Soc.* 132 (2010) 1276–1288, doi:<http://dx.doi.org/10.1021/ja9050444>.
- [8] L. Huang, Y. Chen, B. Liang, B. Xing, G. Wen, S. Wang, X. Yue, C. Zhu, J. Du, X. Bu, A furanyl acryl conjugated coumarin as an efficient inhibitor and a highly selective off-on fluorescent probe for covalent labelling of thioredoxin reductase, *Chem. Commun.* 50 (2014) 6987–6990, doi:<http://dx.doi.org/10.1039/c4cc02119c>.
- [9] M. Peng, Y. Guo, X. Yang, L. Wang, J. An, A highly selective ratiometric and colorimetric chemosensor for cyanide detection, *Dye Pigm.* 98 (2013) 327–332, doi:<http://dx.doi.org/10.1016/j.dyepig.2013.03.024>.
- [10] X. Zhou, X. Lv, J. Hao, D. Liu, W. Guo, Coumarin-indanedione conjugate as a doubly activated Michael addition type probe for the colorimetric and ratiometric fluorescent detection of cyanide, *Dye Pigm.* 95 (2012) 168–173, doi:<http://dx.doi.org/10.1016/j.dyepig.2012.03.025>.
- [11] F. Ge, H. Ye, H. Zhang, B. Zhao, A novel ratiometric probe based on rhodamine B and coumarin for selective recognition of Fe(III) in aqueous solution, *Dye Pigm.* 99 (2013) 661–665, doi:<http://dx.doi.org/10.1016/j.dyepig.2013.06.024>.
- [12] B. Babür, N. Seferoğlu, M. Öcal, G. Sonugur, H. Akbulut, Z. Seferoğlu, A novel fluorescence turn-on coumarin-pyrazolone based monomethine probe for biothiol detection, *Tetrahedron* (2016) 4498–4502, doi:<http://dx.doi.org/10.1016/j.tet.2016.06.008>.

- [13] H. Wang, L.E. Guo, X.M. Li, L. M. Zhang, Q.L. Xu, G. F. Wu, Y. Zhou, J.F. Zhang, Coumarin-based turn-on fluorescence probes for highly selective detection of Pi in cell culture and *Caenorhabditis elegans*, *Dye Pigm.* 120 (2015) 293–298, doi:<http://dx.doi.org/10.1016/j.dyepig.2015.04.031>.
- [14] X.M. Peng, K.V. Kumar, G.L.V. Damu, C.H. Zhou, Coumarin-derived azolyl ethanols: synthesis, antimicrobial evaluation and preliminary action mechanism, *Sci. China Chem.* 59 (2016) 878–894, doi:<http://dx.doi.org/0.1007/s11426-015-0351-0>.
- [15] S. Erbas-Cakmak, F.Pir Cakmak, S. Demirel Topel. T.B. Uyar, E.U. Akkaya, Selective photosensitization through and logic response: optimization of the ph and glutathione response of activatable photosensitizers, *Chem. Commun.* 51 (2015) 12258–12261, doi:<http://dx.doi.org/10.1039/C5CC01261A>.
- [16] I. Simsek Turan, F. Pir-Cakmak, D. Cansen Yildirim, R. Cetin-Atalay, E. U. Akkaya, Near-ir absorbing bodipy derivatives as glutathione-activated photosensitizers for selective photodynamic action, *Chem. Eur. J.* 20 (2014) 16088–16092, doi:<http://dx.doi.org/10.1002/chem.201405450>.
- [17] S. Demirel Topel, G. Turgut Cin, E. U. Akkaya, Near ir excitation of heavy atom free bodipy photosensitizers through the intermediacy of upconverting nanoparticles *Chem. Commun.* 50 (2014) 8896–8899, doi:<http://dx.doi.org/10.1039/C4CC03387F>.
- [18] E. Ertem, A. Bekdemir, A. Atilgan, E. U. Akkaya, Near-ir absorbing bodipy functionalized spions: a potential magnetic nanoplatform for diagnosis and therapy, *Pure Appl. Chem.* 86 (2014) 899–903, doi:<http://dx.doi.org/10.1515/pac-2013-1114>.
- [19] M. Isik; R. Guliyev, S. Kolemen, Y. Altay, B. Senturk, T. Tekinay, E. U. Akkaya, Designing an intracellular fluorescent probe for glutathione: two modulation sites for selective signal transduction, *Org. Lett.* 16 (2014) 3260–3263, doi:<http://dx.doi.org/10.1021/o1501272z>.

- [20] S. Zhou, J. Jia, J. Gao, L. Han, Y. Li, W. Sheng, The one-pot synthesis and fluorimetric study of 3-(20-benzothiazolyl)coumarins, *Dye Pigm.* 86 (2010) 123–128, doi:<http://dx.doi.org/10.1016/j.dyepig.2009.12.005>.
- [21] K.K. Sanap, S.D. Samant, Synthesis of coumarin based fluorescent compounds, *Tetrahedron Lett.* 53 (2012) 5407–5410, doi:<http://dx.doi.org/10.1016/j.tetlet.2012.07.111>.
- [22] A.B. Tathe, N. Sekar, Red-emitting NLO phoric carbazole-coumarin hybrids- Synthesis, photophysical properties and DFT studies, *Dye Pigm.* 129 (2016) 174–185, <http://dx.doi.org/10.1016/j.dyepig.2016.02.026>.
- [23] A.K. Sanap, K.K. Sanap, G.S. Shankarling, Synthesis and photophysical study of novel coumarin based styryl dyes, *Dye Pigm.* 120 (2015) 190–199, <http://dx.doi.org/10.1016/j.dyepig.2015.04.018>.
- [24] A.B. Tathe, V.D. Gupta, N. Sekar, Synthesis and combined experimental and computational investigations on spectroscopic and photophysical properties of red emitting 3-styryl coumarins, *Dye Pigm.* 119 (2015) 49–55, <http://dx.doi.org/10.1016/j.dyepig.2015.03.023>.
- [25] S.B. Phadtare, K.J. Jarag, G.S. Shankarling, Greener protocol for one pot synthesis of coumarin styryl dyes, *Dye Pigm.* 97 (2013) 105–112, <http://dx.doi.org/10.1016/j.dyepig.2012.12.001>.
- [26] S.N. Margar, N. Sekar, Red and near-infrared emitting bis-coumarin analogues based on curcumin framework-synthesis and photophysical studies, *J. Photochem. Photobiol. A Chem.* 327 (2016) 58–70, <http://dx.doi.org/10.1016/j.jphotochem.2016.05.009>.
- [27] A. Parvez, J. Meshram, V. Tiwari, J. Sheik, R. Dongre, M.H. Youssoufi, T. Ben Hadda, Pharmacophores modeling in terms of prediction of theoretical physico-chemical properties and verification by experimental correlations of novel coumarin derivatives

- produced via Betti's protocol, *Eur. J. Med. Chem.* 45 (2010) 4370–4378, doi:<http://dx.doi.org/10.1016/j.ejmech.2010.06.004>.
- [28] A. Arshad, H. Osman, M.C. Bagley, C.K. Lam, S. Mohamad, A.S.M. Zahariluddin, Synthesis and antimicrobial properties of some new thiazolyl coumarin derivatives, *Eur. J. Med. Chem.* 46 (2011) 3788–3794, doi:<http://dx.doi.org/10.1016/j.ejmech.2011.05.044>.
- [29] D. Patel, R. Patel, P. Kumari, N. Patel, In vitro antimicrobial assessment of coumarin-based *s*-triazinyl piperazines, *Med. Chem. Res.* 21 (2012) 1611–1624, doi:<http://dx.doi.org/10.1007/s00044-011-9676-3>.
- [30] G.L.V. Damu, S.F. Cui, X.M. Peng, Q.M. Wen, G.X. Cai, C.H. Zhou, Synthesis and bioactive evaluation of a novel series of coumarin azoles, *Bioorg. Med. Chem. Lett.* 24 (2014) 3605–3608, doi:<http://dx.doi.org/10.1016/j.bmcl.2014.05.029>.
- [31] X.M. Peng, G.L.V. Damu, C.H. Zhou, Current developments of coumarin compounds in medicinal chemistry, *Curr. Pharm. Des.* 19 (2013) 3884–3930, doi:<http://dx.doi.org/10.2174/1381612811319210013>.
- [32] Y. Shi, C.H. Zhou, Synthesis and evaluation of a class of new coumarin triazole derivatives as potential antimicrobial agents, *Bioorg. Med. Chem. Lett.* 21 (2011) 956–960, doi:<http://dx.doi.org/10.1016/j.bmcl.2010.12.059>.
- [33] Y. Shi, C.H. Zhou, X.D. Zhou, R.X. Geng, Q.G. Ji, Synthesis and antimicrobial evaluation of coumarin-based benzotriazoles and their synergistic effects with chloromycin and fluconazole, *Acta Pharm. Sinica.* 46 (2011) 798–810, (in Chinese).
- [34] S.L. Zhang, G.L.V. Damu, L. Zhang, R.X. Geng, C.H. Zhou, Synthesis and biological evaluation of novel benzimidazole derivatives and their binding behavior with bovine serum albumin, *Eur. J. Med. Chem.* 55 (2012) 164–175, doi:<http://dx.doi.org/10.1016/j.ejmech.2012.07.015>.

- [35] X.L. Wang, K. Wan, C.H. Zhou, Synthesis of novel sulfanilamide-derived 1,2,3-triazoles and their evaluation for antibacterial and antifungal activities, *Eur. J. Med. Chem.* 45 (2010) 4631–4639, doi:<http://dx.doi.org/10.1016/j.ejmech.2010.07.031>.
- [36] G.L.V. Damu, Q.P. Wang, H.Z. Zhang, Y.Y. Zhang, J.S. Lv, C.H. Zhou, A series of naphthalimide azoles: Design, synthesis and bioactive evaluation as potential antimicrobial agents, *Sci. China Chem.* 56 (2013) 952–969, doi:<http://dx.doi.org/10.1007/s11426-013-4873-1>.
- [37] H.Z. Zhang, G.L.V. Damu, G.X. Cai, C.H. Zhou, Design, synthesis and antimicrobial evaluation of novel benzimidazole type of Fluconazole analogues and their synergistic effects with Chloromycin, Norfloxacin and Fluconazole, *Eur. J. Med. Chem.* 64 (2013) 329–344, doi:<http://dx.doi.org/10.1016/j.ejmech.2013.03.049>.
- [38] H.Z. Zhang, J.J. Wei, V.K. Kannekanti, S. Rasheed, C.H. Zhou, Synthesis and biological evaluation of novel d-glucose-derived 1,2,3-triazoles as potential antibacterial and antifungal agents, *Med. Chem. Res.* 24 (2015) 182–196, doi:<http://dx.doi.org/10.1007/s00044-014-1123-9>.
- [39] H.D. Ali Paduka, E. K. Paul, G. Thorfinnur, Colorimetric ‘naked-eye’ and fluorescent sensors for anions based on amidourea functionalised 1,8-naphthalimide structures: anion recognition via either deprotonation or hydrogen bonding in DMSO, *New J. Chem.* 32 (2008) 1153–1161, doi:<http://dx.doi.org/10.1039/b715533f>.
- [40] M. Arvind, M. Shahid, P. Dwivedi, An efficient thiourea-based colorimetric chemosensor for naked-eye recognition of fluoride and acetate anions: UV–vis and ¹H NMR studies, *Talanta* 80 (2009) 532–538, doi:<http://dx.doi.org/10.1016/j.talanta.2009.07.020>.
- [41] E.A. Katayev, Y.A. Ustynyuk, L.J. Sessler, Receptors for tetrahedral oxyanions, *Coord. Chem. Rev.* 250 (2006) 3004–3037, doi:<http://dx.doi.org/10.1016/j.ccr.2006.04.013>.

- [42] T. Gunnlaugsson, M. Glynn, G.M. Tocci, P.E. Kruger, F.M. Pfeffer, G.M. Thorfinnur, Anion recognition and sensing in organic and aqueous media using luminescent and colorimetric sensors, *Coord. Chem. Rev.* 250 (2006) 3094–3117, doi:<http://dx.doi.org/10.1016/j.ccr.2006.08.017>.
- [43] S.O. Kang, R.A. Begum, K. Bowman-James, Amide-based ligands for anion coordination, *Angew. Chem. Int. Ed.* 45 (2006) 7882–7894, doi:<http://dx.doi.org/10.1002/anie.200602006>.
- [44] A.P. De Silva, H.N. Gunaratne, T. Gunnlaugsson, A.J. Huxley, C.P. McCoy, J. T. Rademacher, T. E. Rice, Signaling recognition events with fluorescent sensors and switches, *Chem. Rev.* 97(1997), 1515–1566, doi:<http://dx.doi.org/10.1021/cr960386p>.
- [45] A.H. McKie, S. Friedland, F. Hof, Tetrazoles are potent anion recognition elements that emulate the disfavored anti conformations of carboxylic acids, *Org. Lett.* 10 (2008) 4653–4655, doi:<http://dx.doi.org/10.1021/ol801943u>.
- [46] D. Esteban-Gomez, L. Fabbrizzi, M. Licchelli, Why, on interaction of urea-based receptors with fluoride, beautiful colors develop, *Org. Chem.* 70 (2005) 5717–5720, doi:<http://dx.doi.org/10.1021/jo050528s>.
- [47] Y.H. Zhou, P.C. Zheng, X.P. Bao, Selective recognition and discrimination of H₂PO₄⁻ and F⁻ based on a cleft-shaped anion receptor incorporating bisamide and bispyrrole groups, *Supramol. Chem.* 26 (2014) 761–768, doi:<http://dx.doi.org/10.1080/10610278.2013.872243>.
- [48] E.J. Cho, J.W. Moon, S.W. Ko, J.Y. Lee, S.K. Kim, J. Yoon, K.C. Nam, A new fluoride selective fluorescent as well as chromogenic chemosensor containing a naphthalene urea derivative, *J. Am. Chem. Soc.* 125 (2003) 12376–12377, doi:<http://dx.doi.org/10.1021/ja036248g>.

- [49] D.S. Kim, K.H. Ahn, Fluorescence “turn-on” sensing of carboxylate anions with oligothiophene-based *o*-(carboxamido) trifluoroacetophenones, *J. Org. Chem.* 73 (2008) 6831–6834, doi:<http://dx.doi.org/10.1021/jo801178y>.
- [50] T. Gunnlaugsson, A. P. Davis, G. M. Hussey, J. Tierney, Design, synthesis and photophysical studies of simple fluorescent anion PET sensors using charge neutral thiourea receptors, *Org. Biomol. Chem.* 2 (2004) 1856–1863, doi:<http://dx.doi.org/10.1039/B404706K>.
- [51] S.E. García-Garrido, C. Caltagirone, M. E. Light, P. A. Gale, Acridinone-based anion receptors and sensors, *Chem. Commun.* 14 (2007) 1450–1452, doi:<http://dx.doi.org/10.1039/b618072h>.
- [52] J. Shao, A novel colorimetric and fluorescence anion sensor with a urea group as binding site and a coumarin group as signal unit, *Dye Pigm.* 87 (2010) 272–276, doi:<http://dx.doi.org/10.1016/j.dyepig.2010.04.007>.
- [53] D.H. Lee, J.H. Im, S.U. Son, Y.K. Chung, J.I. Hong, An azophenol-based chromogenic pyrophosphate sensor in water, *J. Am. Chem. Soc.* 125 (2003) 7752–7753, doi:<http://dx.doi.org/10.1021/ja034689u>.
- [54] J.Y. Lee, E. J. Cho, S. Mukamel, K. C. Nam, Efficient fluoride-selective fluorescent host: experiment and theory, *J. Org. Chem.* 69 (2004) 943–950, doi:<http://dx.doi.org/10.1021/jo0356457>.
- [55] L. Nie, Z. Li, J. Han, X. Zhang, R. Yang, W. Liu, F. Wu, J. Xie, Y. Zhao, Y. Jiang J., Development of *N*-benzamidothioureas as a new generation of thiourea-based receptors for anion recognition and sensing, *Org. Chem.* 69 (2004) 6449–6454, doi:<http://dx.doi.org/10.1021/jo049088f>.

- [56] B. Liu, T. He, A ratiometric fluorescent chemosensor for fluoride ions based on a proton transfer signaling mechanism, *J. Mater. Chem.* 15 (2005) 2681–2686, doi:<http://dx.doi.org/10.1039/B501234A>.
- [57] R. Nishiyabu, A. Pavel, Sensing of antipyretic carboxylates by simple chromogenic calix[4]pyrroles, *J. Am. Chem. Soc.* 127 (2005) 8270–8271, doi:<http://dx.doi.org/10.1021/ja051421p>.
- [58] R. Martínez-Máñez, F. Sancenón, Fluorogenic and chromogenic chemosensors and reagents for anions, *Chem. Rev.* 103 (2003) 4419–4476, doi:<http://dx.doi.org/10.1021/cr010421e>.
- [59] B. Babür, N. Seferoğlu, Z. Seferoğlu, A ratiometric fluorescence chemosensor based on a coumarin–pyrazolone hybrid: the synthesis and an investigation of the photophysical, tautomeric and anion binding properties by spectroscopic techniques and DFT calculations, *Tetrahedron Lett.* 56 (2015) 2149–2154, doi:<http://dx.doi.org/10.1016/j.tetlet.2015.03.014>.
- [60] W. Huang, Z. Chen, H. Lin, A novel thiourea–hydrazone-based switch-on fluorescent chemosensor for acetate, *J. Lumin.* 131 (2011) 592–596, doi:<http://dx.doi.org/10.1016/j.jlumin.2010.10.036>.
- [61] J. Shao, H. Lin, M. Yu, Z. Cai, H. Lin, Study on acetate ion recognition and sensing in aqueous media using a novel and simple colorimetric sensor and its analytical application, *Talanta* 75 (2008) 551–555, doi:<http://dx.doi.org/10.1016/j.talanta.2007.11.048>.
- [62] U. Yanar, B. Babür, D. Pekyılmaz, I. Yahaya, B. Aydın, Y. Dede, Z. Seferoğlu, A fluorescent coumarin-thiophene hybrid as a ratiometric chemosensor for anions: Synthesis, photophysics, anion sensing and orbital interactions, *J. Mol. Struct.* 1108 (2016) 269–277, doi:<http://dx.doi.org/10.1016/j.molstruc.2015.11.081>.

- [63] Z. Guo, W. Zhu, H. Tian, Dicyanomethylene-4*H*-pyran chromophores for OLED emitters, logic gates and optical chemosensors, *Chem. Commun.*, 2012, 48, 6073–6084, doi:10.1039/c2cc31581e.
- [64] Z. Gao, X. Zhang, Y. Chen, Red fluorescence thin film based on a strong push-pull dicyanoisophorone system, *Dyes Pigm.* 113 (2015) 257–262, doi:http://dx.doi.org/10.1016/j.dyepig.2014.08.014.
- [65] S.N. Margar, N. Sekar, Red and near-infrared emitting bis-coumarin analogues based on curcumin framework-synthesis and photophysical studies, *J. Photochem. Photobiol. A Chem.* 327 (2016) 58–70, doi:http://dx.doi.org/10.1016/j.jphotochem.2016.05.009.
- [66] M. Peng, Y. Guo, X. Yang, L. Wang, J. An, A highly selective ratiometric and colorimetric chemosensor for cyanide detection, *Dye Pigm.* 98 (2013) 327–332, doi:http://dx.doi.org/10.1016/j.dyepig.2013.03.024.
- [67] X. Zhou, X. Lv, J. Hao, D. Liu, W. Guo, Coumarineindanedione conjugate as a doubly activated Michael addition type probe for the colorimetric and ratiometric fluorescent detection of cyanide, *Dye Pigm.* 95 (2012) 168–173, doi:http://dx.doi.org/10.1016/j.dyepig.2012.03.025.
- [68] M.J Frisch, G.W. Trucks, H.B. Schlegel, G.E. Scuseria, M.A. Robb, J.R. Cheeseman, et. al. Gaussian 09, revision A.2. Wallingford CT: Gaussian, Inc.; 2009.
- [69] A.D. Becke, Density-functional exchange-energy approximation with correct asymptotic behavior, *Phys. Rev. A* 38 (1988) 3098–3100, doi:http://dx.doi.org/10.1103/PhysRevA.38.3098.
- [70] A.D. Becke, Density-functional thermochemistry. III. The role of exact exchange, *J. Chem. Phys.* 98 (1993) 5648–5652, doi:http://dx.doi.org/10.1063/1.464913.

- [71] C.T. Lee, W.T. Yang, R.G. Parr, Development of the Colle-Salvetti correlation-energy formula into a functional of the electron density, *Phys. Rev. B* 37 (1988) 785–789, doi:<http://dx.doi.org/10.1103/PhysRevB.37.785>.
- [72] V. Barone, M. Cossi, Quantum calculation of molecular energies and energygradients in solution by a conductor solvent model, *J. Phys. Chem. A* 102 (1998) 1995–2001, doi:<http://dx.doi.org/10.1021/jp9716997>.
- [73] D.R. Kanis, M.A. Ratner, T.J. Marks, Design and Construction of Molecular Assemblies with Large Second-Order Optical Nonlinearities: Quantum Chemical Aspects, *Chem. Rev.* 94 (1994) 195–242, doi:<http://dx.doi.org/10.1021/cr00025a007>.
- [74] D. Lupo, *Molecular Nonlinear Optics: Materials, Physics, and Devices*, J. Zyss (Ed.), Academic Press, San Diego. CA 1994, XIII, 478 pp., hardcover, ISBN 0-12- 784450-3, *Adv. Mater.* 7 (1995) 248–249, <http://dx.doi.org/10.1002/adma.19950070232>.
- [75] S.P. Karna, *Electronic and Nonlinear Optical Materials: The Role of Theory and Modeling*, *J. Phys. Chem. A* 104 (2000) 4671–4673, doi:<http://dx.doi.org/10.1021/jp001296y>.
- [76] J.C. García-Ramos, R. Galindo-Murillo, F. Cortés-Guzmán, L.Ruiz-Azuara, Metal Based Drug-DNA Interactions, *J. Mex. Chem. Soc.* 57 (2013) 245–259, ISSN 1870-249X.

Tables Captions

Table 1. Photophysical properties of the push-pull fluorophores (**CI-1** and **CI-2**) in various solvent.

Table 2. The computed absorption spectra at B3LYP/6-31+G(d,p) for **CI-1** and **CI-2** in different solvents. H and L referred to HOMO and LUMO.

Table 3. Electric dipole moment (μ), polarizability (α_{tot}), molecular first hyperpolarizability (β_{tot}) and their componenets calculated at the B3LYP/6-31+g(d,p) level for **CI-1** and **CI-2**. The components are in a.u.

Table 4. Antimicrobial activity of the compounds expressed as inhibition zones (mm).

Table 5. MIC and MFK values of the compounds (μM).

Scheme Captions

Scheme 1. Synthetic pathway of **CI-1** and **CI-2**.

Scheme 2. Proposed binding mode of **CI-1** with F^- in DMSO solution.

Figure Captions

Fig. 1. Absorption (top, **CI-1**, left **CI-2**, right, $c=3\times 10^{-5}$ M) and emission (bottom, **CI-1**, left **CI-2**, right, $c=3\times 10^{-7}$ M) spectra of the dyes **CI-1** and **CI-2** in DMSO.

Fig. 2. Color changes in day light (top, **CI-1**, left **CI-2**, right, $c=3\times 10^{-5}$ M) and upon UV irradiation (365 nm) (bottom, **CI-1**, left **CI-2**, right, $c=3\times 10^{-5}$ M).

Fig. 3. The absorption spectra of **CI-1** ($c=2\times 10^{-5}$ M) upon addition of F^- , AcO^- and CN^- ($c=1\times 10^{-2}$ M) in DMSO.

Fig. 4. Photographs of **CI-1** ($c=2 \times 10^{-5}$ M in DMSO) upon addition of 20 equiv studied anions ($c=1 \times 10^{-2}$ M in DMSO) under ambient light.

Fig.5. Absorption spectra of **CI-1** ($c=2 \times 10^{-5}$ M) in the presence of F^- (40 equiv) upon addition of increasing amount of TFA (40 equiv) in DMSO.

Fig. 6. The absorption spectra of **CI-1** ($c=2 \times 10^{-5}$ M) upon addition of F^- , AcO^- and CN^- ($c=1 \times 10^{-2}$ M) in DMSO/ H_2O (9:1).

Fig. 7. Photographs of **CT-1** ($c=2 \times 10^{-5}$ M in DMSO/ H_2O (9:1)) upon addition of 20 equiv of F^- , AcO^- and CN^- ($c=1 \times 10^{-5}$ M in DMSO) under ambient light.

Fig. 8. The absorption spectra of **CI-2** ($c=2 \times 10^{-5}$ M) upon addition of CN^- ($c=1 \times 10^{-2}$ M) in DMSO.

Fig. 9. Photographs of **CI-2** ($c=2 \times 10^{-5}$ M in DMSO) upon addition of 20 equiv of F^- , AcO^- and CN^- ($c=1 \times 10^{-5}$ M in DMSO) under ambient light.

Fig.10. 1H -NMR (300 MHz) spectra taken over the course of the titration of a DMSO- d_6 solution of **CI-1** ($c=1 \times 10^{-2}$ M) with a standard DMSO solution F^- .

Fig.11. 1H -NMR (300 MHz) spectra taken over the course of the titration of a DMSO- d_6 solution of **CI-1** ($c=1 \times 10^{-2}$ M) with a standard DMSO solution CN^- .

Fig.12. 1H -NMR (300 MHz) spectra taken over the course of the titration of a DMSO- d_6 solution of **CI-2** ($c=1 \times 10^{-2}$ M) with a standard DMSO solution CN^- .

Fig.13. The optimized structures of a) **CI-1**, b) **CI-2**, c) **CI-1**+ F^- , d) **CI-1**+ AcO^- .

Fig.14. Molecular orbitals of the relevant excitations for **CI-1**, **CI-1**+ F^- and **CI-1**+ AcO^- .

Fig. 15. Molecular electrostatic potential map for **CI-1** and **CI-2** calculated at the B3LYP/6-31+G(d,p) level.

Fig.16. TGA curves of **CI-1** and **CI-2**.

Fig. 17. The electrophoretograms applied to the incubated mixtures of DNA at various concentrations (lane 1: $c=150 \times 10^{-6}$ M, lane 2: $c=75 \times 10^{-6}$ M, lane 3: $c=37.5 \times 10^{-6}$ M, lane 4: $c=18.75 \times 10^{-6}$ M, lane 5: $c=9.37 \times 10^{-6}$ M, lane 6: $c=4.69 \times 10^{-6}$ M) of the compounds **CI-1** (1-6) and **CI-2** (1-6).

Fig. 18. The electrophoretogram for the *Bam*HI and *Hind*III digested mixtures of plasmid DNA after the treatment with the compounds **CI-1** (Lanes 1-3) and **CI-2** (Lanes 4-6).

Table 1. Photophysical properties of the push-pull fluorophores (**CI-1** and **CI-2**) in various solvent.

CI-1					CI-2				
Solvents	$\lambda_{\text{abs,max}}$ (nm)	$\log \epsilon$ ($\text{cm}^{-1}\text{M}^{-1}$)	$\lambda_{\text{em,max}}$ (nm)	Stokes shifts (nm)	Solvents	$\lambda_{\text{abs,max}}$ (nm)	$\log \epsilon$ ($\text{cm}^{-1}\text{M}^{-1}$)	$\lambda_{\text{em,max}}$ (nm)	Stokes shifts (nm)
CH ₂ Cl ₂	446,391(s)	4.69	587	141	CH ₂ Cl ₂	461,385(s)	4.72	583	122
Dioxan	444	4.59	556	112	Dioxan	452,372(s)	4.66	568	116
DMF	387(s),466,528(s)	4.58	545	79	DMF	471,389(s)	4.79	539	68
DMSO	470,397(s)	4.68	547	77	DMSO	477,401(s)	4.69	555	78
THF	447,380(s)	4.60	576	129	THF	455,378(s)	4.73	584	129

Table 2. The computed absorption spectra at B3LYP/6-31+G(d,p) for **CI-1** and **CI-2** in different solvents. H and L referred to HOMO and LUMO.

CI-1				CI-2		
	λ_{max} (nm)	Oscillator strength, f	Orbital contributions	λ_{max} (nm)	Oscillator strength, f	Orbital contributions
CH ₂ Cl ₂	439	0.7250	H-1→L (96%)	447	0.7584	H-1→L (96%)
	378	0.5842	H→L+1 (73%)	377	0.5294	H→L+1 (95%)
Dioxan	434	0.6614	H-1→L (95%)	441	0.6657	H-1→L (76%)
	368	0.4849	H→L+1 (93%)	368	0.5507	H→L+1 (63%)
DMF	441	0.7449	H-1→L (96%)	449	0.7847	H-1→L (96%)
	380	0.5889	H→L+1 (90%)	380	0.5110	H→L+1 (95%)
DMSO	441	0.7430	H-1→L (96%)	448	0.7833	H-1→L (96%)
	380	0.5863	H→L+1 (90%)	380	0.5067	H→L+1 (95%)
THF	438	0.7156	H-1→L (96%)	446	0.7473	H-1→L (96%)
	377	0.5541	H→L+1 (61%)	376	0.5287	H→L+1 (94%)

Table 3. Electric dipole moment (μ), polarizability (α_{tot}), molecular first hyperpolarizability (β_{tot}) and their components calculated at the B3LYP/6-31+g(d,p) level for **CI-1** and **CI-2**. The components are in a.u.

	CI-1	CI-2		CI-1	CI-2
α_{xx}	653.69	673.28	β_{xxx}	3898.10	2536.96
α_{xy}	-19.65	-23.96	β_{xxy}	5460.58	6191.06
α_{yy}	439.79	471.82	β_{xyy}	-1687.70	-1663.43
α_{xz}	15.02	15.45	β_{yyy}	961.30	794.53
α_{yz}	-2.60	-4.18	β_{xxz}	212.84	216.44
α_{zz}	233.13	242.24	β_{xyz}	-221.13	-225.22
$\alpha_{\text{tot}} (10^{-24})$ (esu)	65.60	68.50	β_{yyz}	201.83	183.26
μ_x	-2.26	1.85	β_{xzz}	-296.92	-258.23
μ_y	-4.51	-4.92	β_{yzz}	-109.12	-161.89
μ_z	-1.81	-1.76	β_{zzz}	-146.53	-153.76
μ (D)	13.6	14.10	$\beta_{\text{tot}} (10^{-30})$ (esu)	57.0	59.20

Table 4. Antimicrobial activity of the compounds expressed as inhibition zones (mm).

Test microorganisms	Compounds		Positive control		
	CI-1	CI-2	Amp	C	Keto
<i>E. coli</i> ATCC 35218	10±1	-	-	8 ± 0	NS
<i>E. coli</i> ATCC 25922	8±2	-	18 ± 0	25 ± 0	NS
<i>B. cereus</i> NRRL B-3711	-	-	-	-	NS
<i>B. subtilis</i> ATCC 6633	-	-	23 ± 1	21 ± 0	NS
<i>S. aureus</i> ATCC 25923	-	-	44 ± 1	24 ± 1	NS
<i>E. faecalis</i> ATCC 29212	-	-	27 ± 0	20 ± 0	NS
<i>P. aeruginosa</i> ATCC 27853	8±1	-	60 ± 0	34 ± 0	NS
<i>K. pneumoniae</i> ATCC 13883	9±1	-	-	31 ± 1	NS
<i>S. typhimurium</i> ATCC 14028	10±2	8±1	19 ± 1	38 ± 1	NS
<i>E. hirae</i> ATCC 9790	-	-	9 ± 1	22 ± 1	NS
<i>P. vulgaris</i> RSKK 96029	-	-	-	32 ± 1	NS
<i>C. albicans</i> ATCC 10231	16±7	14±1	NS	NS	11 ± 1
<i>C. krusei</i> ATCC 6258	-	20±1	NS	NS	18 ± 1
<i>C. tropicalis</i> Y-12968	-	14±1	NS	NS	34 ± 2

Amp: Ampicillin, C: Chloramphenicol, Keto: Ketokanazol (NS: Not studied)

Table 5. MIC and MFC values of the compounds (μM).

Test microorganisms	MIC		MFC	
	CT-1	CT-2	CT-1	CT-2
<i>C. albicans</i> ATCC 10231	10 μM	20 μM	80 μM	80 μM
<i>C. krusei</i> ATCC 6258	20 μM	20 μM	20 μM	20 μM
<i>C. tropicalis</i> Y-12968	20 μM	20 μM	20 μM	20 μM

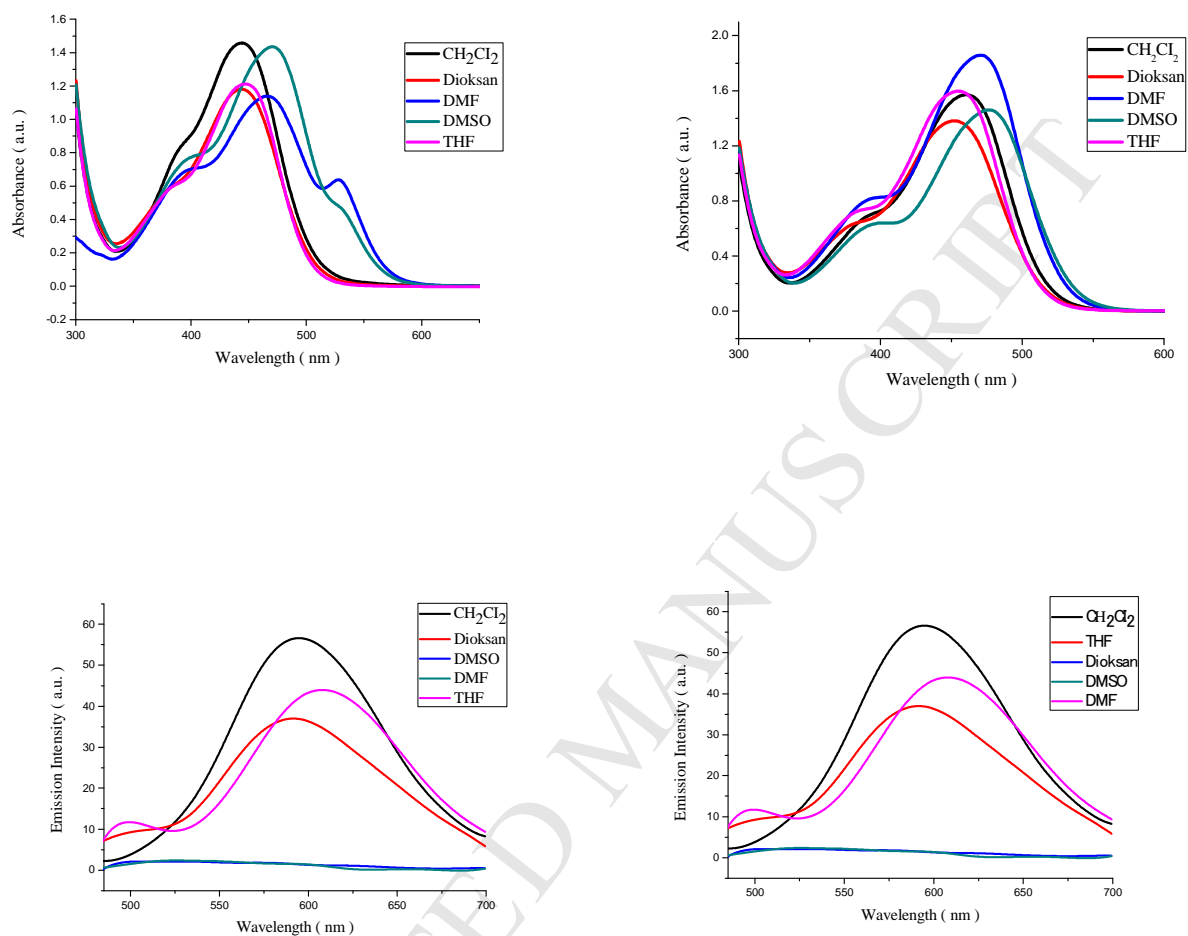


Fig. 1. Absorption (top, **CI-1**, left **CI-2**, right, $c=3 \times 10^{-5}$ M) and emission (bottom, **CI-1**, left **CI-2**, right, $c=3 \times 10^{-7}$ M) spectra of the dyes **CI-1** and **CI-2** in DMSO.

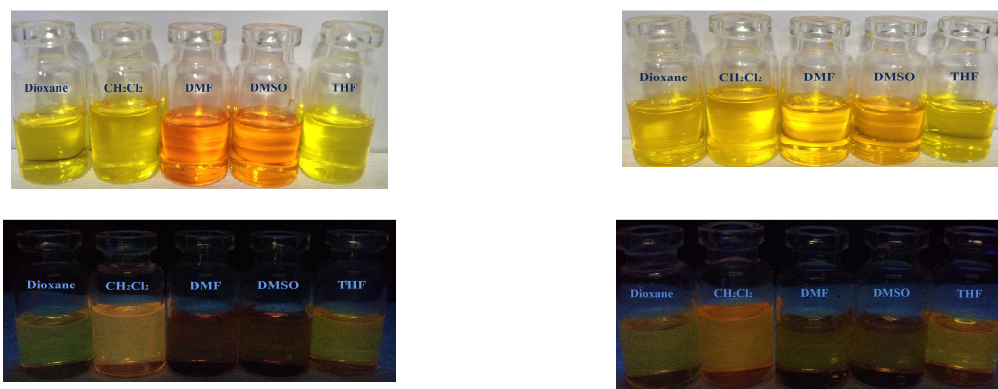


Fig. 2. Color changes in day light (top, **CI-1**, left **CI-2**, right, $c=3\times 10^{-5}$ M) and upon UV irradiation (365 nm) (bottom, **CI-1**, left **CI-2**, right, $c=3\times 10^{-5}$ M).

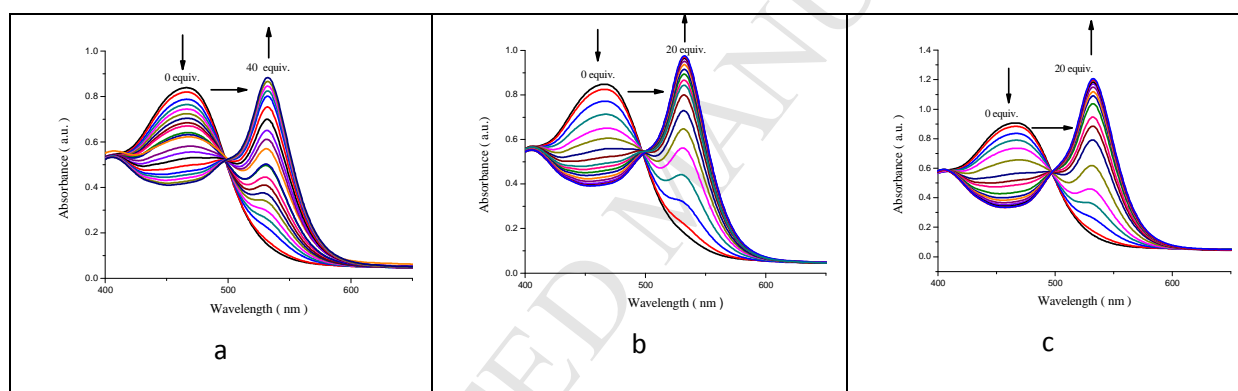


Fig. 3. The absorption spectra of **CI-1** ($c=2\times 10^{-5}$ M) upon addition of F⁻, AcO⁻ and CN⁻ ($c=1\times 10^{-2}$ M) in DMSO.



Fig. 4. Photographs of **CI-1** ($c=2\times 10^{-5}$ M in DMSO) upon addition of 20 equiv studied anions ($c=1\times 10^{-2}$ M in DMSO) under ambient light.

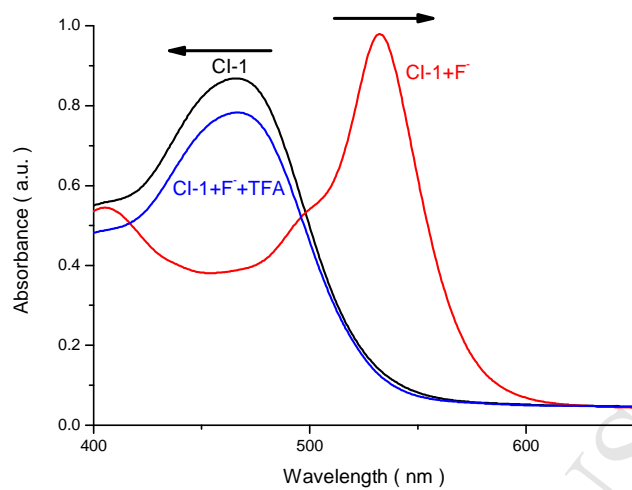


Fig.5. Absorption spectra of **CI-1** ($c=2\times 10^{-5}$ M) in the presence of F^- (40 equiv) upon addition of increasing amount of TFA (40 equiv) in DMSO.

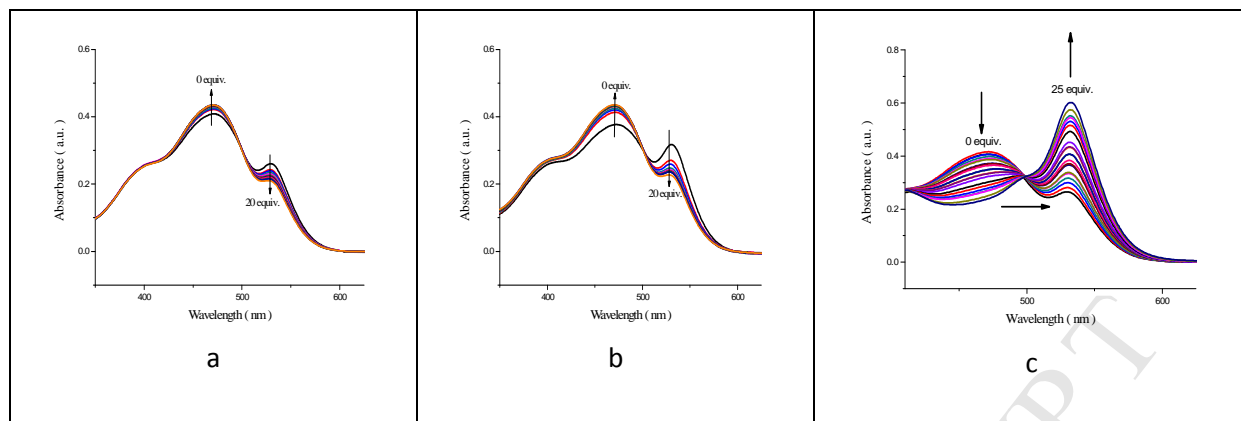


Fig. 6. The absorption spectra of **CT-1** ($c=2 \times 10^{-5}$ M) upon addition of F⁻, AcO⁻ and CN⁻ ($c=1 \times 10^{-2}$ M) in DMSO/H₂O (9:1).



Fig. 7. Photographs of **CT-1** ($c=2 \times 10^{-5}$ M in DMSO/H₂O (9:1)) upon addition of 20 equiv of F⁻, AcO⁻ and CN⁻ ($c=1 \times 10^{-5}$ M in DMSO) under ambient light.

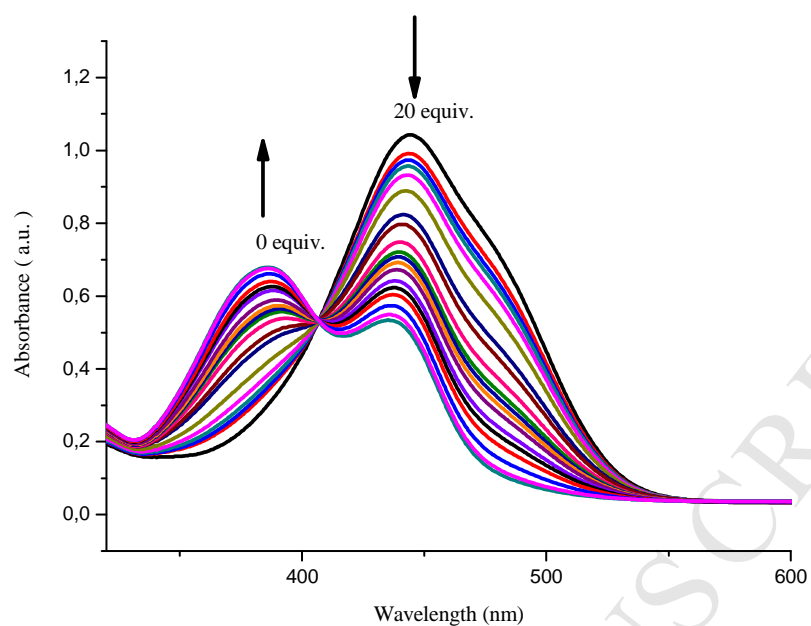


Fig. 8. The absorption spectra of **CI-2** ($c=2\times 10^{-5}$ M) upon addition of 20 equiv of CN^- ($c=1\times 10^{-2}$ M) in DMSO.



Fig. 9. Photographs of **CI-2** ($c=2\times 10^{-5}$ M in DMSO) upon addition of 20 equiv of F^- , AcO^- and CN^- ($c=1\times 10^{-5}$ M in DMSO) under ambient light.

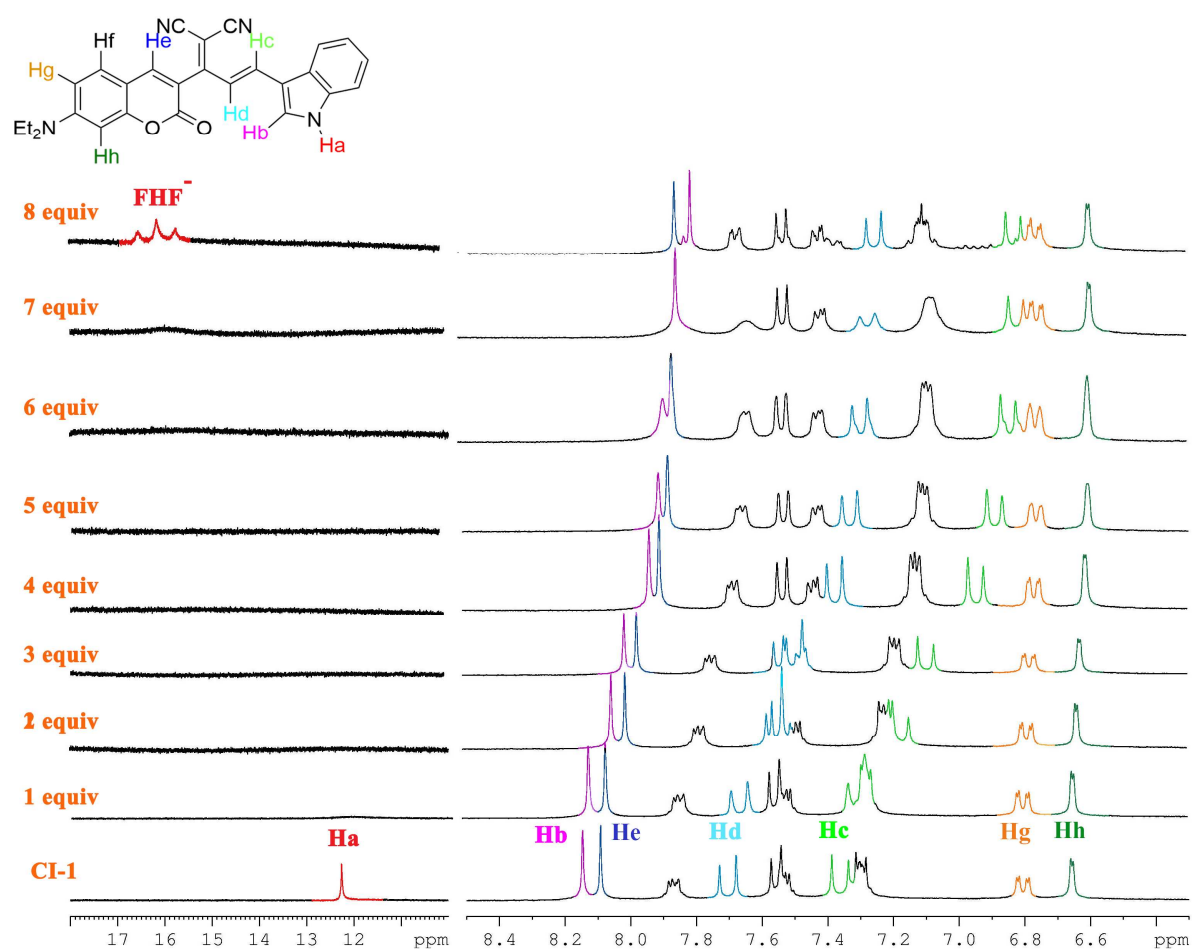


Fig.10. ¹H-NMR (300 MHz) spectra taken over the course of the titration of a DMSO-*d*₆ solution of CI-1 ($c=1 \times 10^{-2}$ M) with a standard DMSO solution F⁻.

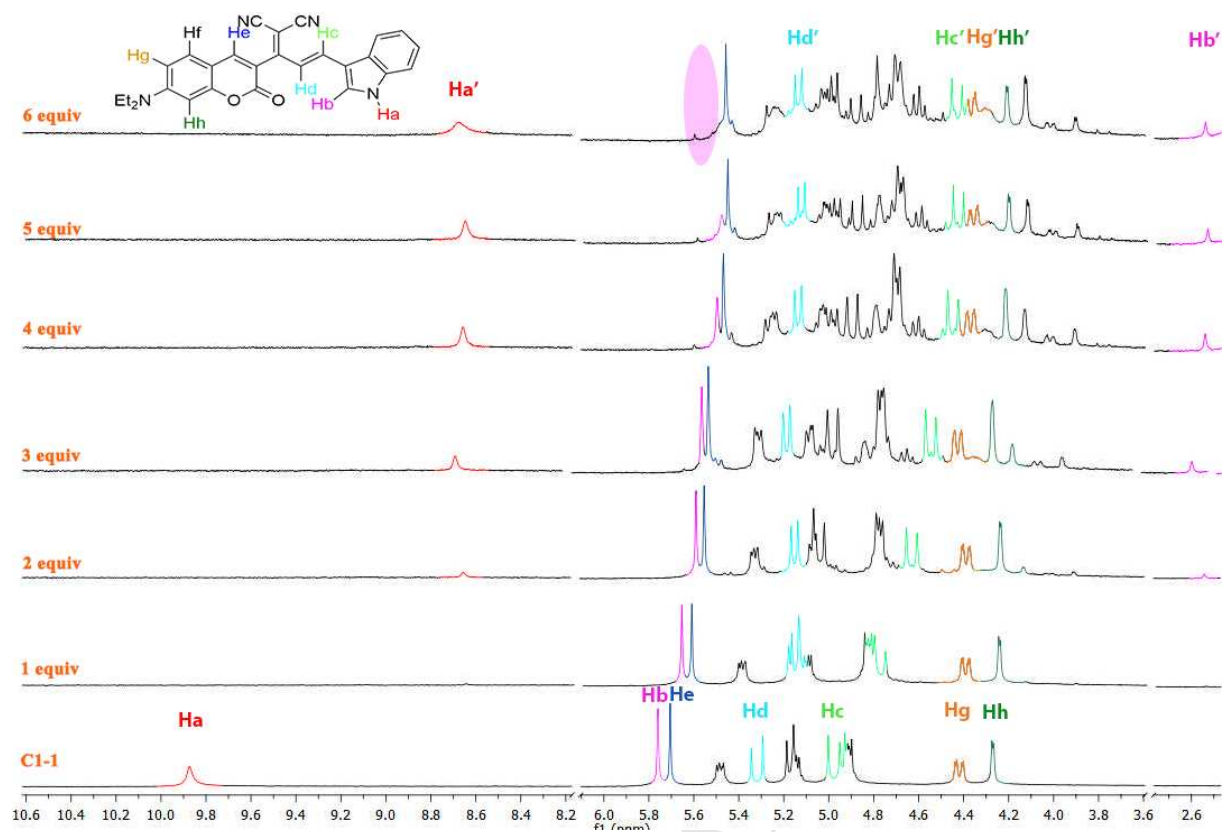


Fig.11. ¹H-NMR (300 MHz) spectra taken over the course of the titration of a DMSO-*d*₆ solution of **CI-1** ($c=1 \times 10^{-2}$ M) with a standard DMSO solution of CN⁻.

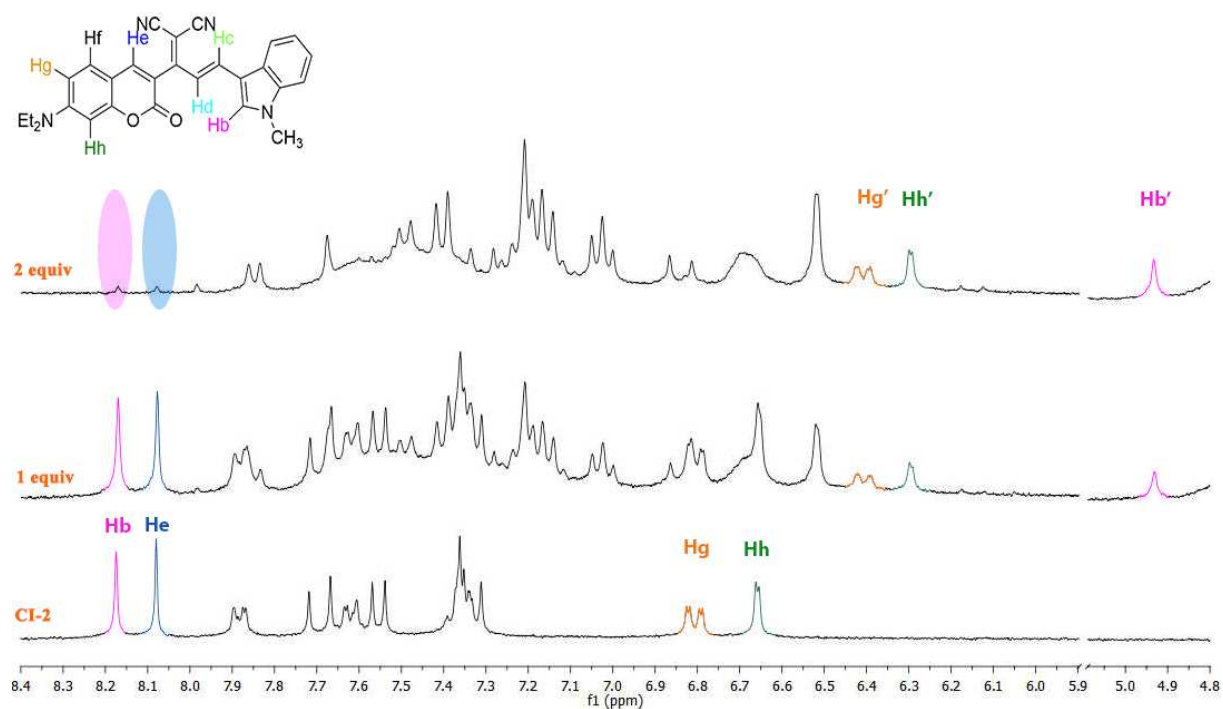


Fig.12. $^1\text{H-NMR}$ (300 MHz) spectra taken over the course of the titration of a $\text{DMSO-}d_6$ solution of CI-2 ($c=1 \times 10^{-2} \text{ M}$) with a standard DMSO solution of CN^- .

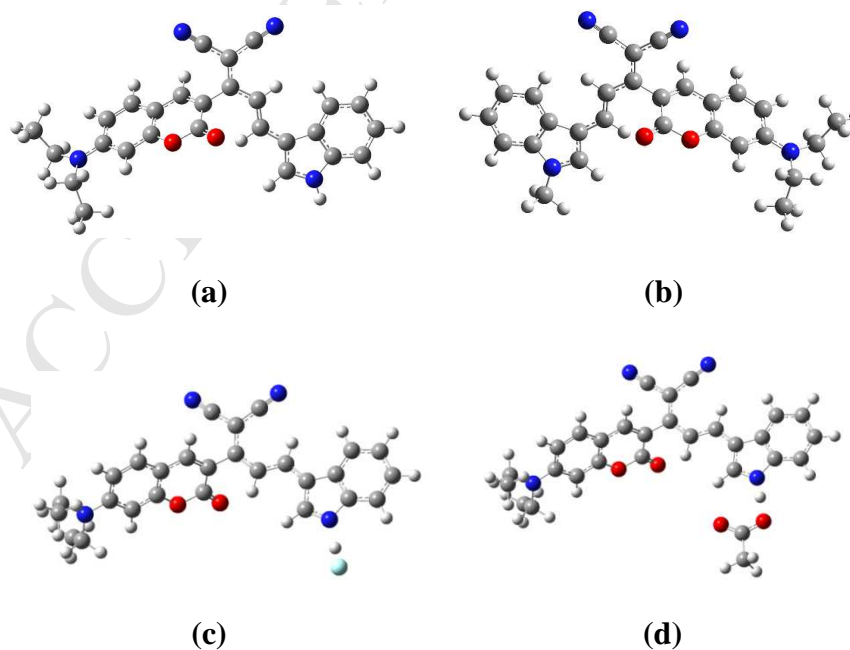


Fig.13. The optimized structures of a) CI-1, b) CI-2, c) CI-1 + F^- , d) CI-1 + AcO^- .

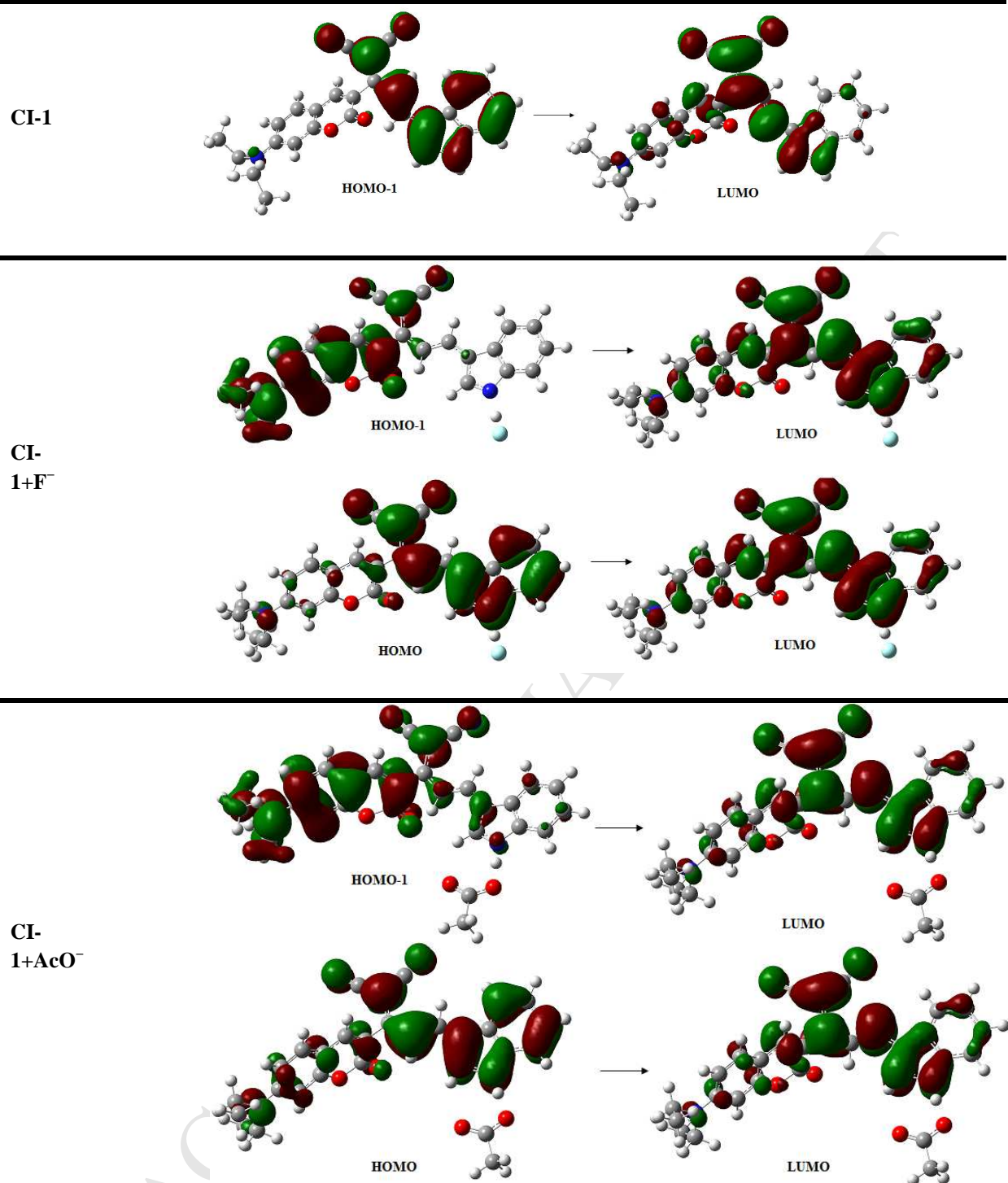


Fig.14. Molecular orbitals of the relevant excitations for CI-1, CI-1+F⁻ and CI-1+AcO⁻.

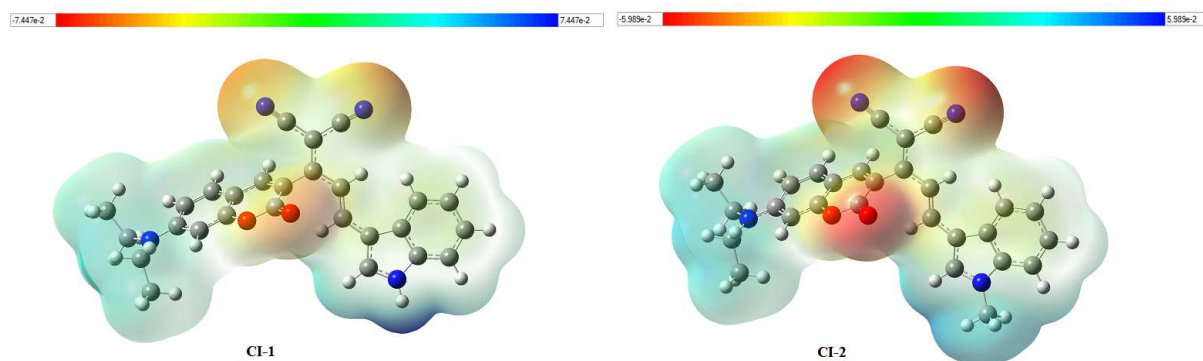


Fig. 15. Molecular electrostatic potential map for **CI-1** and **CI-2** calculated at the B3LYP/6-31+G(d,p) level.

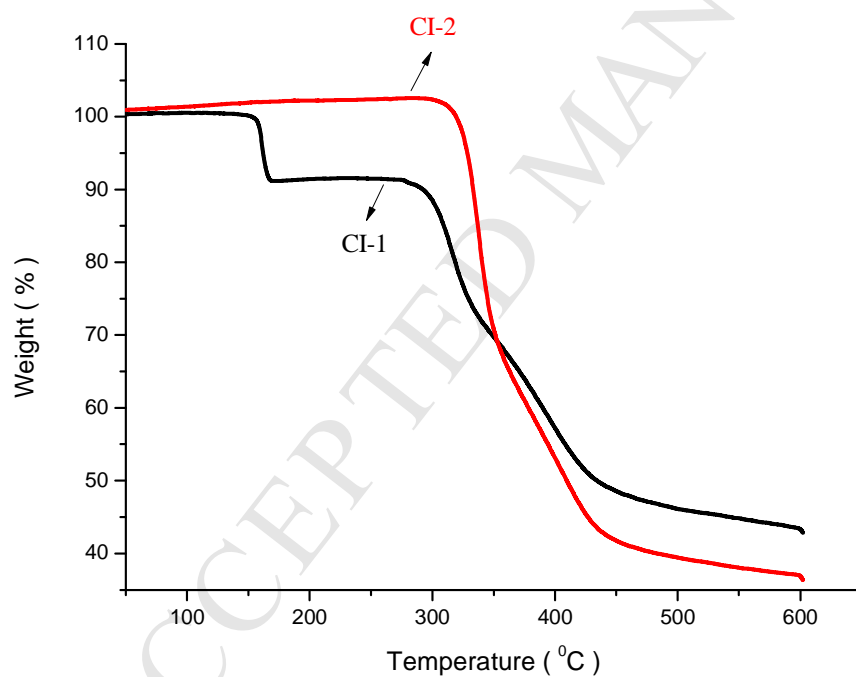


Fig.16. TGA curves of **CI-1** and **CI-2**.

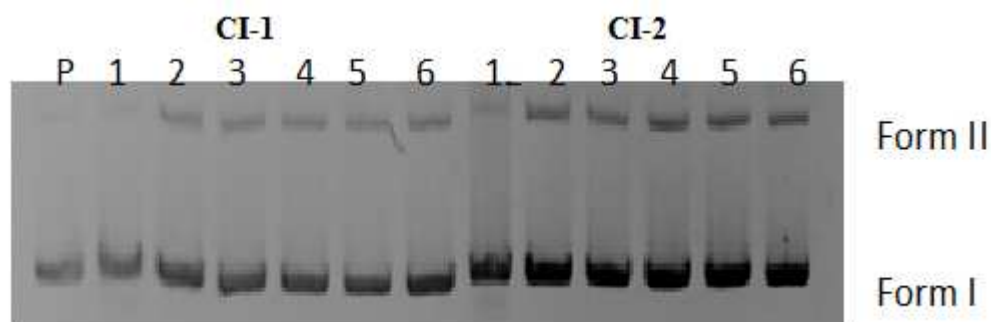
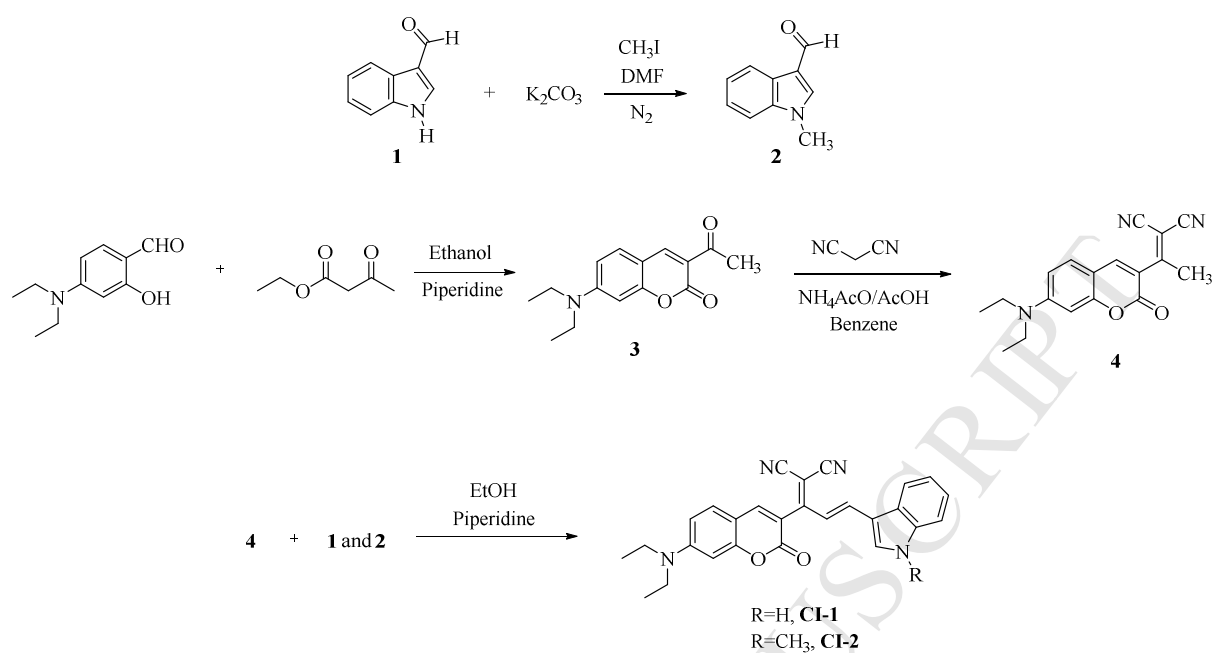


Fig. 17. The electrophoretograms applied to the incubated mixtures of DNA at various concentrations (lane 1: $c=150\ \mu\text{M}$, lane 2: $c=75\ \mu\text{M}$, lane 3: $c=37.5\ \mu\text{M}$, lane 4: $c=18.75\ \mu\text{M}$, lane 5: $c=9.37\ \mu\text{M}$, lane 6: $c=4.69\ \mu\text{M}$) of the compounds **CI-1** (1-6) and **CI-2** (1-6).



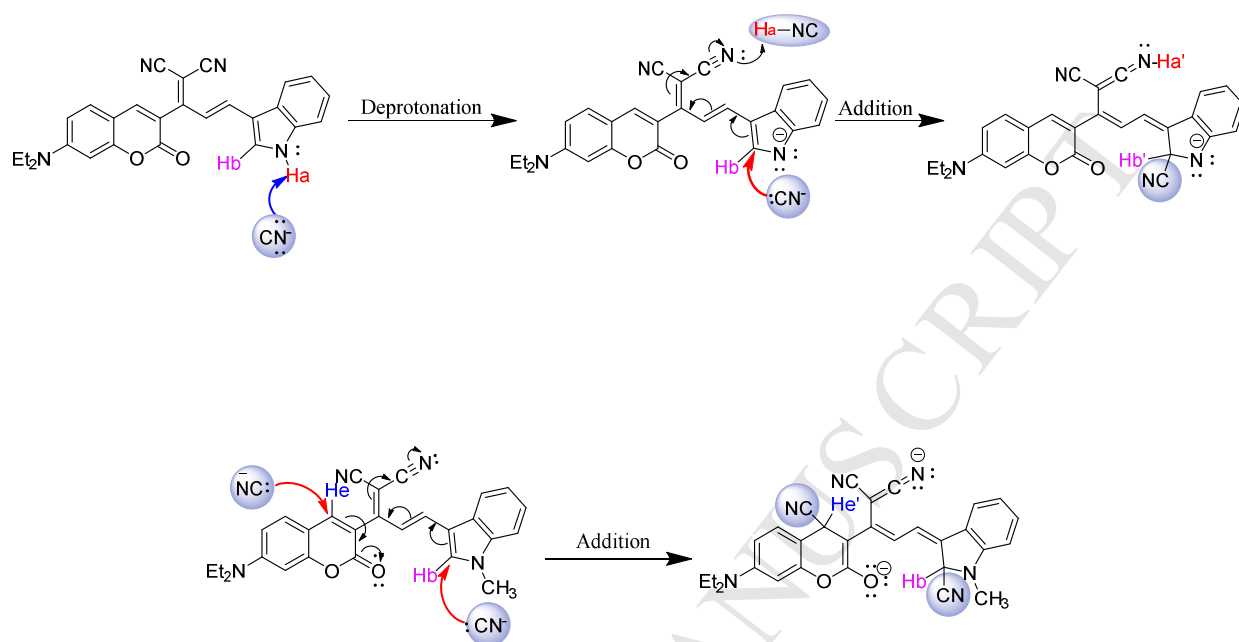
Fig. 18. The electrophoretogram for the *Bam*HI and *Hind*III digested mixtures of plasmid DNA after the treatment with the compounds **CI-1** (Lanes 1-3) and **CI-2** (Lanes 4-6).



Scheme 1. Synthetic pathway of **CI-1** and **CI-2**.



Scheme 2. Proposed binding mode of **CI-1** with F^- in DMSO solution.



Scheme 3. Proposed binding mode of **CI-1** (top) and **CI-2** (bottom) with CN⁻ via addition and deprotonation mechanisms in DMSO solution.

Highlights

- Two new coumarin-indole conjugate fluorescent dyes (**CI-1** and **CI-2**) having donor-acceptor-donor (D-A-D) were synthesized and characterized.
- **CI-1** and **CI-2** behave as a colorimetric probe for selective and sensitive detection of CN^- in DMSO/ H_2O (9:1) and DMSO, respectively.
- They showed good thermal stability for practical applications as functional dye.
- The both dyes cause conformational changes on DNA and bind to selectively nucleotides of A/A and G/G.